

How Far Are Vision-Language Models from Constructing the Real World? A Benchmark for Physical Generative Reasoning

Luyu Yang Yutong Dai An Yan Viraj Prabhu Ran Xu Zeyuan Chen
Salesforce AI Research

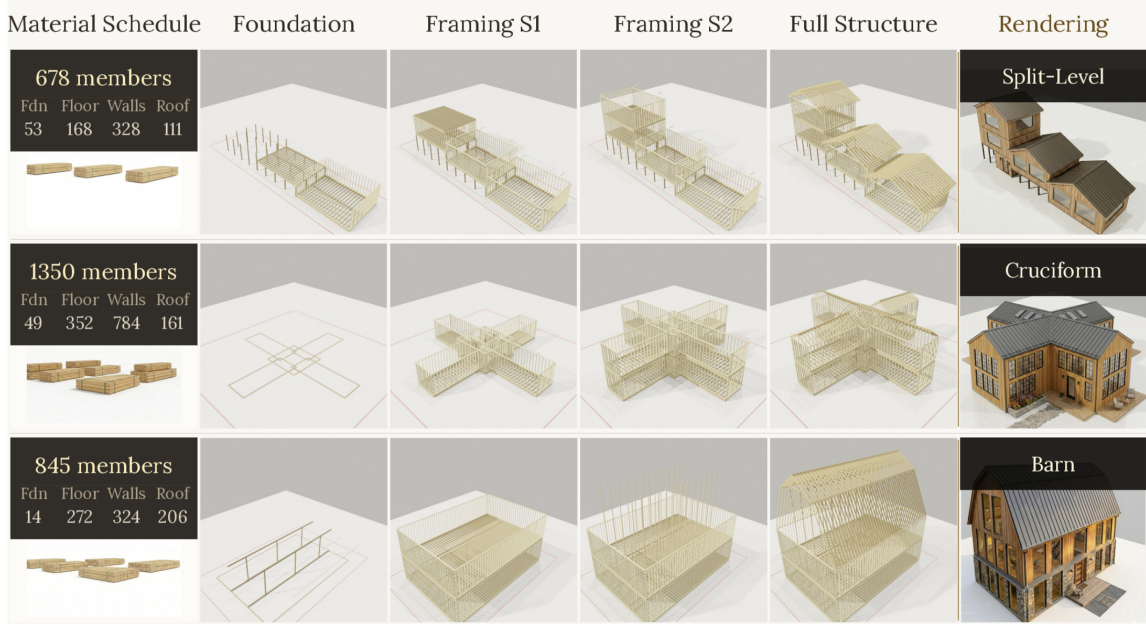


Figure 1. **DreamHouse benchmark samples.** Each row shows a single structure across five representations: material schedule (member counts by subsystem), foundation, two intermediate framing stages, and complete timber frame, alongside the target exterior rendering from which the model must infer the hidden structural system. Three of the 13 architectural styles are shown: Split-Level (678 members), Cruciform (1,350 members), and Barn (845 members). Member counts span four subsystems: foundation (Fdn), floor, walls, and roof.

Abstract

The physical world is not merely visual; it is governed by rigorous structural and procedural constraints. Yet, the evaluation of vision-language models (VLMs) remains heavily skewed toward perceptual realism, prioritizing the generation of visually plausible 3D layouts, shapes, and appear-

*ances. Current benchmarks rarely test whether models grasp the step-by-step processes and physical dependencies required to actually build these artifacts—a capability essential for automating design-to-construction pipelines. To address this, we introduce **DreamHouse**, a novel benchmark for physical generative reasoning: the capacity to synthesize artifacts that concurrently sat-*

isfy geometric, structural, constructability, and code-compliance constraints. We ground this benchmark in residential timber-frame construction, a domain with fully codified engineering standards and objectively verifiable correctness. We curate over 26,000 structures spanning 13 architectural styles—each verified to construction-document standards (LOD 350)—and develop a deterministic 10-test structural validation framework. Unlike static benchmarks that assess only final outputs, DreamHouse supports iterative agentic interaction. Models observe intermediate build states, generate construction actions, and receive structured environmental feedback, enabling a fine-grained evaluation of planning, structural reasoning, and self-correction. Extensive experiments with state-of-the-art VLMs reveal substantial capability gaps that are largely invisible on existing leaderboards. These findings establish physical validity as a critical evaluation axis orthogonal to visual realism, highlighting physical generative reasoning as a distinct and underdeveloped frontier in multimodal intelligence. Available at <https://luluyuyuyang.github.io/dreamhouse>

1. Introduction

The physical world is not merely a surface; it is a rigorous system of constraints [11, 29, 31, 32, 38, 41, 45, 52]. A floor must bear load, a rafter must respect its allowable span, and a wall must continuously transfer force from roof to foundation. These are not aesthetic choices, but fundamental physical realities. Yet, the dominant evaluation paradigm for generative vision models treats the world as purely visual, asking only if a model can produce outputs that *look* ‘correct’ [6, 16, 18, 24, 42, 44]. Whether those outputs could physically *stand* is a question the field has largely left unasked.

While the recent surge in vision-language models (VLMs) has yielded remarkable perceptual capabilities, evaluating their grasp of physical laws remains in its infancy [13, 14, 35, 44, 53]. Recent benchmarks like PhysBench [14] and VSI-Bench [13] probe physical reasoning and spatial recall, but they are fundamentally *comprehension*

tasks—the model observes, answers, and is scored. They do not evaluate whether a model can *build*. Generating a physically realizable artifact from scratch, under strict engineering constraints and without visible ground truth, requires moving beyond passive observation. Between perceiving a structure and constructing one lies a critical gap that standard benchmarks fail to measure.

To bridge this gap, we introduce **DreamHouse**, a novel benchmark designed to evaluate **physical generative reasoning**—the capacity to synthesize artifacts that concurrently satisfy geometric, structural, and code-compliance constraints. We ground our benchmark in residential timber-frame construction. This domain provides fully codified correctness criteria and discrete, verifiable components, while remaining visually complex enough to prove that perceptual plausibility alone is insufficient. DreamHouse comprises over 26,000 structurally verified models spanning 13 architectural styles. Furthermore, we provide a suite of 10 deterministic, physics-based tests covering load paths, span limits, member connectivity, *etc.*. Crucially, these tests operate directly on the scene graph, bypassing the need for computationally expensive simulations.

The DreamHouse task is formulated as an iterative generation process: given rendered views of a target structure, a model must generate Blender Python construction code, process structured validation feedback, and refine its output until all structural tests pass. We evaluate performance across three protocols with varying degrees of external scaffolding (Planner-Atomic, Planner-Reactive and Planner-Managed) and two input conditions (bare framing visible, *Frame*, versus occluded by finished cladding, *Facade*). This framework serves as a controlled ablation study, isolating whether generation failures stem from weak spatial reasoning, deficient planning, or an inability to self-correct.

Our extensive evaluation of three frontier VLMs including GPT-5 [37], Gemini 3 [2] and Claude 4.5 [1] across more than 20,000 independent agentic tasks reveals striking limitations in current state-of-the-art models. Notably, models that excel on standard coding and reasoning leaderboards often

struggle with physical generation; highly-ranked generalists frequently underperform compared to their peers when evaluated under our structured protocols. Even the most capable model achieves a joint pass rate of **merely 7.1%**, successfully satisfying both structural validity and visual fidelity simultaneously. These findings demonstrate that physical generative reasoning is not a natural byproduct of general intelligence, but rather a distinct, underdeveloped capability axis demanding dedicated evaluation. Our contributions:

- **Physical generative reasoning** as a novel VLM evaluation axis, distinct from perception, comprehension, and simulation-based benchmarks.
- **The DreamHouse benchmark**, comprising 26,000+ verified timber-frame structures across 13 architectural styles with multi-view renderings and construction phase-wise annotations.
- **A 10-test structural validation suite** that is deterministic and simulation-free, covering International Residential Code (IRC) compliance [15], physics, geometry, and fabrication details.
- **A three-protocol agentic evaluation framework**, showing that scaffold design is as important as model selection for physical generation tasks.

2. Related Work

Physical and Spatial Benchmarking for VLMs.

A growing body of work exposes systematic gaps between VLM semantic fluency and physical-world grounding [13, 14, 23, 34, 35, 53]. Phys-Bench [14] evaluates 75 VLMs on 10K video-image-text entries spanning object properties, relationships, and dynamics, finding that models excel at static recognition but fail on Newtonian dynamics, a deficiency attributed to missing physical priors rather than perceptual limits. VSI-Bench [48] measures metric visual-spatial intelligence (distances, sizes, directions) from egocentric video, showing that standard chain-of-thought prompting *degrades* spatial estimation, models must instead build explicit cognitive maps. Think-with-3D [13] endows VLMs with 3D geometric imagination via latent alignment and RL-based spatial rewards, enabling occluded geometry completion from sparse

views. These benchmarks evaluate *passive* physical understanding: answering questions about or reconstructing observed scenes. DreamHouse targets the harder *generative* gap, producing structures that are themselves physically valid, without any reference structure to recall.

3D Scene Generation. Large-scale 3D generative models [6, 18, 24, 27, 42, 44, 54] optimize photometric or geometric metrics against reference renderings, leaving structural validity unmeasured. TRELIS [47] achieves state-of-the-art image-conditioned 3D generation via sparse voxel latents, but its representation is derived entirely from visual observations, a generated house mesh may score well on Chamfer distance while failing every structural test. SpatialGen [19] generates photorealistic indoor scenes conditioned on 3D layouts, operating at rendering-grade level-of-detail for design visualization. DreamHouse operates at fabrication-grade detail (LOD 350), specifying member species, cross-sections, and connections sufficient for construction scheduling, complementary positions in the AEC pipeline.

Code-Driven Structured Generation. A productive line of work [12, 17, 39, 40, 50, 55] has VLMs write executable programs verified by domain-specific oracles, consistently outperforming direct pixel-level synthesis for structured outputs. DreamHouse adopts this architecture but replaces the visual oracle with deterministic engineering compliance. VIGA [51] frames inverse graphics as a long-horizon agentic loop (WRITE→RUN→RENDER→COMPARE→REVISE), demonstrating that iterative execution feedback recovers performance where single-shot VLMs fail. Its feedback signal is photometric; structural failures (missing members, span violations) are invisible to any rendering oracle. BlenderGym [21] benchmarks VLMs on Blender editing tasks via LPIPS/CLIP-I, sharing our infrastructure but evaluating visual imitation rather than structural correctness. MCP-Universe [28] benchmarks LLM agents across six domains including 3D Design, where even GPT-5 achieves only 43.7% success; DreamHouse provides the domain-specific 16-test physical validation absent from its 3D tasks. Auto-

Present [20] and Chart2Code [40] further confirm that programmatic generation dominates pixel-level synthesis for structured outputs; DreamHouse extends this finding to 3D structural engineering where constraints are physical law rather than aesthetic convention.

Physically-Grounded Assembly. The works closest to DreamHouse require agents to produce physical assemblies whose validity is determined by physics, not appearance [9, 26, 43]. BrickGPT [34] is the most directly analogous: it formulates LEGO assembly as next-token prediction with physics-aware rollback, explicitly framing its contribution as “buildable, not just renderable.” The technical gap is substantial: LEGO involves isotropic material with uniform stud connectivity and a single stability check (center-of-mass within support polygon), whereas timber framing involves orthotropic material, heterogeneous connection mechanics, and multi-condition verification (load-path connectivity, section modulus compliance, IRC span limits, assembly dependency ordering). Beyond domain complexity, BrickGPT [34] is a trained generation method; DreamHouse is an evaluation benchmark. Video2Policy [49] instantiates the same visual-to-executable-program paradigm for robotic manipulation, representing a complementary instance of visual-to-physical program synthesis in a distinct physical domain.

3. DreamHouse Benchmark

We construct **DreamHouse**, a benchmark for physical generative reasoning grounded in residential timber-frame construction. It comprises (1) a large-scale dataset of structurally verified structures paired with multi-view renderings, and (2) a deterministic validation suite of 10 physics-based tests scoring any generated structure against engineering and code-compliance standards [15, 33]. Together they define both the task and the metric, enabling objective evaluation of whether a model can *construct*, not merely depict, the physical world.

3.1. Benchmark Construction

Testbed choice. Residential timber framing is an unusually well-suited domain for evaluating phys-

ical generative reasoning: its correctness criteria are fully codified (load-path integrity, member sizing, connection geometry, assembly order) and objectively verifiable without human annotation [46]. The domain is also visually rich and stylistically diverse, making perceptual plausibility a meaningful but insufficient criterion. Before this choice, we piloted an alternative **bridge-generation** testbed but found that frontier VLMs could easily satisfy all validation tests by recovering a small set of geometric parameters analytically from the image, bypassing structural understanding entirely; *see Appendix for details*. Timber framing forecloses this shortcut: member spacing, connection hierarchy and load-path topology are not directly legible from exterior renders, and no analytic inversion exists.

Parametric generation and dataset scale. Each structure originates from a JSON configuration defining footprint dimensions, story count, roof pitch, overhang depth. A procedural Blender Python generator instantiates this into a fully resolved 3D timber-frame model with human in the loop — individual foundation sills, floor joists, wall studs, headers, ridge beams, rafters, and collar ties, each at the correct position, orientation, and IRC cross-section, with member identities and parent-child relationships preserved in a structured scene graph.

We identify **13 canonical residential styles** [25] whose structural logic is sufficiently distinct to stress different aspects of the reasoning pipeline: *A-Frame, Barn, Carriage, Colonial, Courtyard, Cruciform, Farmhouse, Ranch, Saltbox, Shotgun, Split-Level, Townhouse, and Z-Plan*. These span single- and multi-story footprints, symmetric and asymmetric roofs, and rectangular to complex multi-wing plans (Figure 2 and Figure 1). After filtering through the full validation suite, the released dataset contains **26,543 provably buildable structures**, ranging from 133 to 1,548 members (mean 673, median 656), partitioned into Foundation, Floor, Walls, and Roof categories [5]. All structures are rendered from five canonical viewpoints using Blender [22] Cycles. All structures meet **LoD 350** (fabrication-grade); *see Appendix for de-*

Dataset Statistics: Member Count and Style Distribution

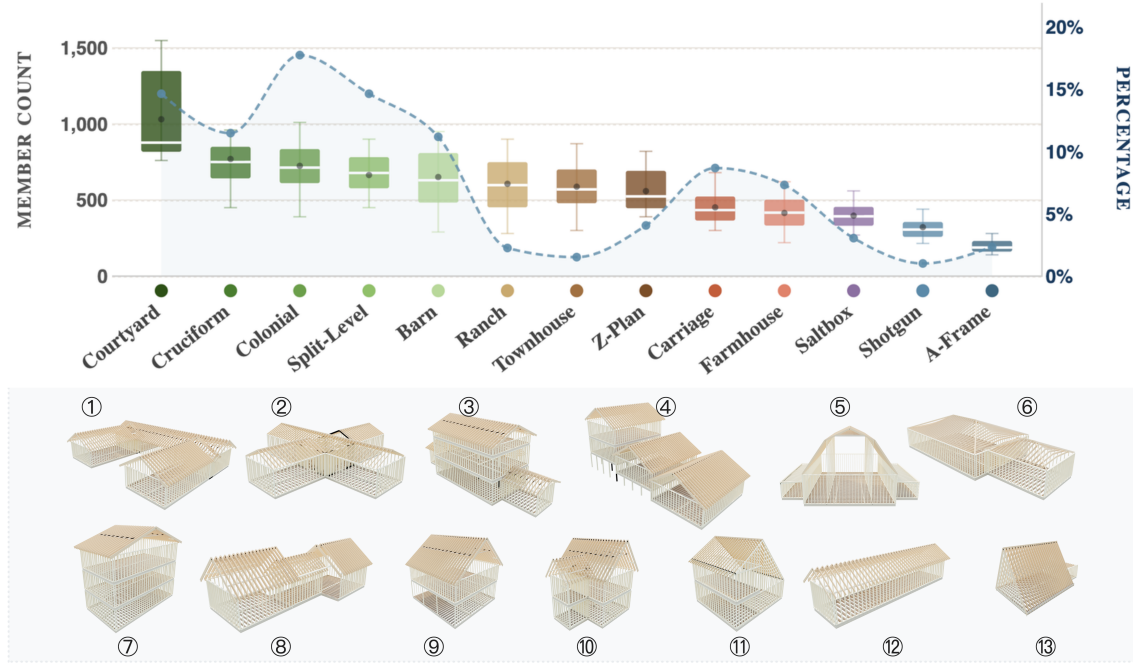


Figure 2. **DreamHouse Dataset Overview.** (Top) Dataset statistics showing member count distributions (box plots, left axis) and style proportions (dashed line, right axis) across all **13** architectural styles, ordered by decreasing structural complexity. Member counts range from 133 to 1,548 (mean 673). (Bottom) Representative Cycles-rendered timber frame structures for each style: *Courtyard*, *Cruciform*, *Colonial*, *Split-Level*, *Barn*, *Ranch*, *Townhouse*, *Z-Plan*, *Carriage*, *Farmhouse*, *Saltbox*, *Shotgun*, *A-Frame*, spanning complex multi-wing configurations to compact single-story forms.

tails.

Structural Validation Suite. The suite comprises 10 deterministic tests in three pillars operating directly on the scene graph. With no physics simulation required, our evaluation can be fast, deterministic, and interpretable (Figure 3); *full mathematical definitions are provided in Appendix.*

3.2. Task Formalization

We formalize evaluation as a family of *agentic generation tasks*. Let \mathcal{A} denote the agent (VLM), \mathcal{E} the executor (Blender environment), and \mathcal{V} the structural validator. At each turn t , \mathcal{A} receives observation $o_t = (I_0, f_{t-1})$, where I_0 is the fixed multi-

view task input and f_{t-1} is structured validation feedback from the previous turn, and produces a Blender Python action a_t . \mathcal{E} applies a_t to transition the scene graph $s_{t-1} \rightarrow s_t$, and \mathcal{V} evaluates s_t to produce feedback f_t reporting per-test pass/fail status and violation counts (e.g., “*Beam-Post gap exceeds 3.0m; detected spacing 7.0m between BeamPost_01 and rim*”). This feedback closes the loop: f_t becomes part of o_{t+1} . On failure, the agent retries from the same scene state s_t without resetting context; the full conversation history $\mathcal{H}_t = (I_0, a_1, f_1, \dots, a_{t-1}, f_{t-1})$ is preserved across all retries. Before writing any code, \mathcal{A} produces a hierarchical JSON plan specifying member categories, phase ordering, and assembly

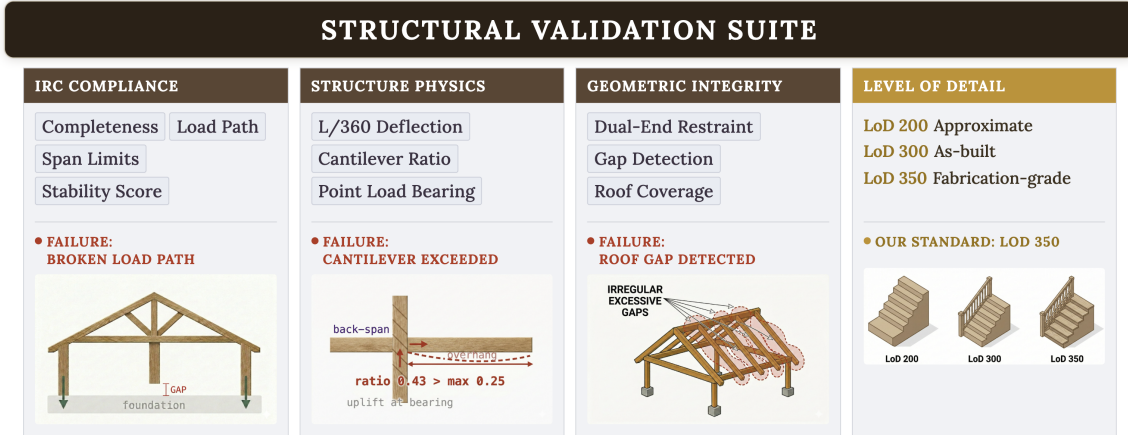


Figure 3. **Structural Validation Suite**. 10 tests across four pillars. **IRC Compliance** (left): load path, span limits, completeness, stability score. **Structure Physics** (center-left): L/360 deflection, cantilever ratio, point load bearing. **Geometric Integrity** (center-right): dual-end restraint, gap detection, roof coverage. **LoD 350** (right): fabrication-grade member geometry.

dependencies. Each task enforces a per-step retry budget R_{step} and a global budget R_{global} .

We instantiate three protocols that vary the degree of external phase management, forming a controlled ablation over agentic scaffold design. The same deterministic validation suite \mathcal{V} used to certify benchmark structures during dataset construction serves as the evaluation signal during task execution, ensuring ground-truth and assessment criteria are fully aligned.

Planner-Atomic (\mathcal{T}_S). \mathcal{A} receives $o_1 = (I_0, \emptyset)$ and generates a complete construction script a_1 covering all member categories in a single code block. On failure, a_t is regenerated from updated \mathcal{H}_t ; accepted when $\mathcal{V}(s_t)$ passes all 10 tests or R_{global} is exhausted. This protocol tests holistic single-pass structural synthesis with no intermediate feedback between phases.

Planner-Reactive (\mathcal{T}_Q). \mathcal{A} generates a single script covering all K construction phases in a self-determined order. After each phase k is materialized into s_t , it is evaluated against $\mathcal{V}_{\text{mid}} \subset \mathcal{V}$ (load path and stability); failure triggers full script regeneration from \mathcal{H}_t , invalidating all phases

$k+1, \dots, K$. Unlike \mathcal{T}_S , the model must re-plan all phase interdependencies in context after each failure — combining the demands of holistic planning and sequential commitment without any external scaffolding.

Planner-Managed (\mathcal{T}_W). \mathcal{A} generates scripts one phase at a time under external phase management. The scene s_t persists across phases; each phase must pass \mathcal{V}_{mid} before the next is unlocked, with up to R_{step} retries per phase. A failure at phase k never invalidates s_{t-1} : only a_t is regenerated, leaving all prior scene state intact. This protocol provides the strongest external scaffolding and isolates each phase as an independent sub-task.

Iterative Refinement with Visual Feedback (\mathcal{T}_E). Beyond the core generation protocols, we introduce an exploratory editing task to test whether models can refine visual alignment without breaking an already valid structure. Starting from s_T that passed \mathcal{V} under \mathcal{T}_S but achieved visual fidelity score $S < \tau$ (see Section 3.3), \mathcal{A} iteratively refines s_t while preserving structural validity. Feedback f_t is augmented with a rendered side-by-side comparison against the target; \mathcal{V} is re-run at every iteration and

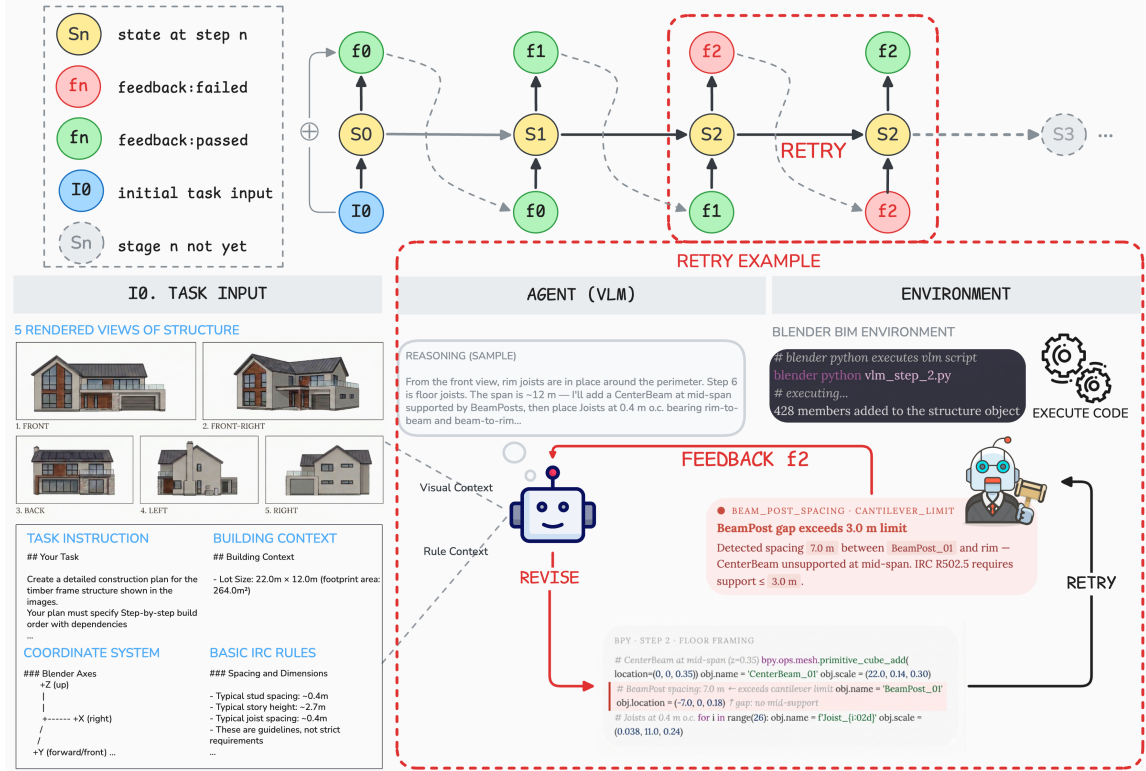


Figure 4. **Task formalization example Planner-Managed.** *Top (agent loop):* Evaluation is formalized as a recurrent agentic process. At each turn t , the agent \mathcal{A} (VLM) receives observation $o_t = (I_0, f_{t-1})$, the original multi-view task image I_0 and structured validation feedback f_{t-1} from the previous turn, and generates a Blender Python action a_t . The executor \mathcal{E} applies a_t to transition the scene graph $s_{t-1} \rightarrow s_t$, and the validator \mathcal{V} produces feedback f_t reporting per-test pass/fail and violation counts. This feedback becomes the input observation for the next turn, closing the loop. On failure (e.g., f_2 , red), the agent retries from the same scene state s_2 without resetting context. \mathcal{A} , \mathcal{E} , and \mathcal{V} are omitted from the diagram for visual clarity; see Section 3.2 for full formalization. *Bottom (task instantiation):* The task input I_0 consists of five rendered views of the target structure paired with building context and rules. The agent reasons over these to produce and iteratively revise construction code; the environment executes the code in Blender and the validator returns structured diagnostic feedback driving the next revision.

any a_t causing structural regression is rejected even if S improves.

3.3. Evaluation Metrics

Structural Validity. This metric axis is binary: a structure either satisfies all tests in \mathcal{V} or it does not. We deliberately avoid partial credit here. Physical constraints are discontinuous by nature, a single unrestrained member or one over-spanned joist renders the assembly unsafe regardless of how well

the rest is built, and a graded score would obscure this harshness. over all N evaluated structures per condition.

Visual Fidelity. We measure pixel-level agreement between multi-view renders of the generated and target structures (Eq.(1)). Standard perceptual embeddings such as DINO or CLIP are ill-suited here: they are trained to be invariant to the geometric and positional differences that matter most

	TARGET	step 1	step 2	step 3	step 4	step 5	step 6	...	step 12
Gemini 3 flash								✓	
Claude 4.5 opus								✓	
GPT 5									

Figure 5. **Planner-Managed qualitative example AF-01-0060 (A-frame style)**. All three models begin from scratch and receive stepwise visual feedback toward the same target structure. Despite reaching a valid result at step 6, **Gemini** and **Claude** employ markedly different construction strategies. Gemini pursues a top-down, shape-first approach: it approximates the overall silhouette early and refines toward it. Claude reasons bottom-up: it first establishes a structurally sound interior frame, then lays the roof rafters over it in the final step – a sequence closer to how a builder would physically construct an A-frame. **GPT-5** fails to recognize the defining constraint of A-frame geometry, that the roof planes double as load-bearing walls, and from step 6 onward enters a false loop of adding conventional wall studs along the perimeter. Unable to escape this structural misconception, it exhausts all attempts without producing a valid result. This example highlights that identical visual feedback can elicit fundamentally different reasoning strategies, and that success depends not just on visual matching ability but on implicit architectural knowledge.

in construction (a wall shifted by 0.5 m looks semantically similar but is structurally wrong), and they provide no signal on missing or misplaced members that happen to fall outside the salient region. We instead use alpha-weighted MSE. Let \hat{R}_v and R_v be the rendered and target images of timber frames at view v , with union alpha mask $m_v = \alpha_v^g \cup \alpha_v^r$ restricting comparison to non-transparent regions of either structure. The visual fidelity score is:

$$S = \frac{1}{V} \sum_{v=1}^V \max \left(0, 1 - \lambda \cdot \frac{\sum_p m_v(p) e_v(p)}{\sum_p m_v(p)} \right) \quad (1)$$

averaged over V orthographic views. The union mask penalizes missing geometry, a member absent in the generated structure leaves unmatched non-transparent pixels in the target without rewarding empty background agreement. Visual fidelity is computed on structurally passed structures only.

Topological Fidelity. Visual similarity can be gamed: a model that generates the correct silhouette but with wrong member counts, misplaced connections, or incorrect spatial hierarchy will score well visually while producing an unbuildable structure (Eq.(2)). We therefore measure structural correspondence directly on the scene graph, independent of rendering, via three complementary statistics: Census accuracy C , Hungarian match rate M , and Voxel IoU V .

C measures whether the model generates the correct number of members per category. Let n_k^* and \hat{n}_k be the ground-truth and generated member counts for category $k \in \{1, \dots, K\}$; then $C = \frac{1}{K} \sum_k \min(n_k^*, \hat{n}_k) / \max(n_k^*, \hat{n}_k)$. This catches global over- or under-building even when individual member positions look plausible, a failure mode that positional metrics miss.

M measures whether individual members are placed at the correct spatial positions. Let σ^* be the optimal assignment from the Hungarian algo-

rithm between ground-truth and generated member centroids $\{c_i\}$ and $\{\hat{c}_j\}$; then $M = \frac{1}{N} \sum_i \mathbf{1}[\|c_i - \hat{c}_{\sigma^*(i)}\| \leq \delta]$ where $\delta = 0.3$ m is the positional tolerance, chosen to be permissive of minor placement error while rejecting members shifted by more than a stud spacing. M catches misalignment even when counts are correct, a failure mode C cannot detect. V measures volumetric overlap of the assembled structure. Let \mathcal{G} and $\hat{\mathcal{G}}$ be the voxelized scene graphs at a fixed grid resolution; then $V = |\mathcal{G} \cap \hat{\mathcal{G}}|/|\mathcal{G} \cup \hat{\mathcal{G}}|$. V catches gross shape errors, e.g. missing wings, wrong footprint extent, collapsed roof geometry that member-level statistics miss because they operate on individual centroids rather than the assembled volume.

The composite score is:

$$T = w_C C + w_M M + w_V V, \quad w_C + w_M + w_V = 1 \quad (2)$$

where $w_M > w_C = w_V$, reflecting that positional match is the most direct measure of assembly correctness, with count accuracy and volumetric overlap contributing equally as complementary diagnostics. Specific weight values are provided in Section 4.

4. Experiments

Models. We evaluate three frontier vision-language models: **GPT-5** [37], **Gemini 3 Flash** [2], **Claude Opus 4.5** [1]. All models use identical prompting with no fine-tuning. We abbreviate Claude Opus 4.5 and Gemini 3 Flash as **Claude** and **Gemini** respectively for brevity.

Evaluation subset. We evaluate on a stratified sample of 1,200 structures per model-protocol cell, drawn uniformly across all 13 styles and 4 roof types, each structure represents a full agentic task: a multi-turn conversation of up to ~ 50 API calls depending on protocol. Across three models and our three main protocols, this yields **21,600** independent agentic tasks and ~ 200 k API calls. Token consumption is correspondingly substantial, totalling approximately **~ 5 B tokens** across the benchmark. This scale reflects the real computa-

tional cost of evaluating frontier models on physically grounded generative tasks.

Details. Visual fidelity uses $V = 5$ orthographic views (front, front-right, back, left, right) at 512×512 with scale factor $\lambda = 10$, mapping a 10% mean pixel error to $S = 0$ and passing threshold $\tau = 0.6$, which corresponds empirically to structures visually recognizable as matching the target style and layout. Topological fidelity is computed with positional tolerance $\delta = 0.3$ m (permissive of minor placement error while rejecting members shifted by more than a stud spacing) and composite weights $w_C = 0.3$, $w_M = 0.4$, $w_V = 0.3$, reflecting that positional match is the most direct measure of assembly correctness (see Appendix for parameter choice). Both visual and topological scores are computed on structurally passed structures only; the joint pass rate J fraction satisfying \mathcal{V} and $S \geq \tau$ simultaneously serves as the primary scalar summary of overall generation quality.

4.1. Main Results

We evaluate each model under two input conditions: *Frame*, in which the model receives a bare timber framing image and must generate a structurally valid assembly, and *Facade*, in which the framing is occluded by finished exterior cladding and the model must infer the underlying structure from appearance alone. Intuitively, the *Facade* condition presents a more challenging task, as it requires the model to solve an inverse problem of hallucinating hidden, load-bearing topologies based solely on superficial exterior cues. Table 1 reports structural pass rates, visual and topological fidelity, and joint pass rates under three agentic generation tasks mentioned in 3.2. Results reveal four cross-cutting patterns that together characterize the current frontier of physically grounded generative reasoning. We detail each observation O in turn.

O1: Structural validity and visual fidelity are orthogonal.

GPT-5 leads structurally in Planner-Atomic (79.2%) yet scores lowest visually

Table 1. Consolidated Performance Metrics for GPT-5, Claude Opus 4.5, and Gemini 3 Flash. *Frame* = bare timber framing; *Facade* = finished exterior. **Bold** = best per column; **shaded rows** = best model per protocol by average across all conditions. **Structural Pass Rate** in $[0, 1]$: passes only if all 16 validation tests clear. **Visual Fidelity**: average visual similarity score across 5 rendered views. **Topological Fidelity**: structural similarity across member counts, spatial alignment, and volumetric overlap. **Joint Pass Rate** in $[0, 1]$: fraction satisfying *both* structural and visual criteria simultaneously.

Model	Protocol	Structural Pass Rate		Visual Fidelity		Topological Fidelity		Joint Pass Rate	
		Frame	Facade	Frame	Facade	Frame	Facade	Frame	Facade
GPT-5	Planner-Atomic	0.792	0.637	0.312	0.287	0.143	0.151	0.035	0.019
	Planner-Reactive	0.302	0.247	0.293	0.266	0.141	0.143	0.003	0.003
	Planner-Managed	0.333	0.157	0.179	0.175	0.178	0.157	0.008	0.003
Claude	Planner-Atomic	0.716	0.779	0.406	0.377	0.164	0.168	0.071	0.064
	Planner-Reactive	0.428	0.494	0.239	0.245	0.133	0.141	0.003	0.013
	Planner-Managed	0.713	0.737	0.278	0.291	0.205	0.190	0.031	0.022
Gemini	Planner-Atomic	0.454	0.539	0.376	0.394	0.171	0.170	0.031	0.036
	Planner-Reactive	0.507	0.376	0.345	0.342	0.160	0.152	0.019	0.013
	Planner-Managed	0.785	0.737	0.313	0.282	0.232	0.211	0.043	0.026

Table 2. Iterative refinement with visual feedback. Each model starts from its Planner-Atomic structural passes and iterates up to 10 visual-feedback revisions. *Baseline* = oneshot output before revision; *Final* = last attempt; *Best* = highest-scoring attempt across all iterations. Δ is Final–Baseline mean score. *Improved Tasks* = fraction of tasks that improved their visual fidelity score. *Structures Retained* = fraction retaining structural validity at the final attempt. **Bold** = best per column.

Model	Mean Visual Score			Δ	% Improved Tasks	Structures Retained
	Baseline	Final	Best			
Claude	0.408	0.441	0.461	+0.033	70.3%	68.5%
GPT-5	0.392	0.405	0.425	+0.013	61.4%	78.1%
Gemini	0.433	0.443	0.471	+0.010	56.1%	73.8%

(0.312); Claude leads visually (0.406) but not structurally; Gemini leads structurally under Planner-Managed (78.5%) while remaining competitive visually (0.313). Models frequently satisfy validation by converging to a generic, physically safe assembly that ignores visual conditioning entirely. Physical validity is not a byproduct of visual imitation, and vice versa.

O2: Structural reasoning is not a monolithic capability.

Although GPT-5 leads structurally in Planner-Atomic (79.2%), it collapses under Planner-

Managed (33.3%), dropping 46 points; Gemini reverses this entirely (45.4% \rightarrow 78.5%), gaining 33 points; Claude is comparably protocol-stable (71.6% vs. 71.3%). We interpret this as two distinct reasoning modes: *holistic* (e.g., GPT-5 is strong single-pass synthesis, weak under incremental commitment) and *Planner-Managed* (e.g., Gemini is strongest with phase decomposition and intermediate feedback). Planner-Reactive experiment confirms this: forcing models to self-decompose a structure into sequential steps without any external phase guidance is harder, as it demands both holistic planning and incremental commitment simultaneously.

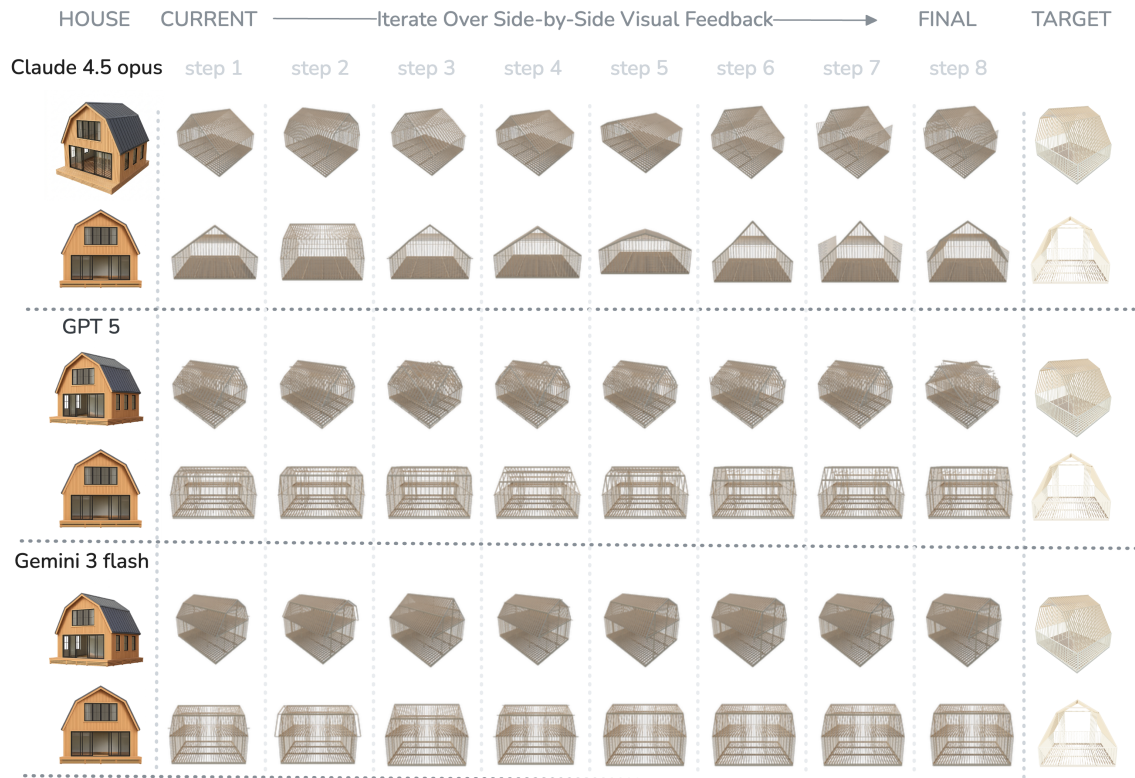


Figure 6. **Iterative Refinement with Visual Feedback (Section 4.2, qualitative example BN-01-0273 (barn style).** Starting from a structurally valid Planner-Atomic output, each model receives up to 10 rounds of side-by-side visual feedback (current render vs. target) and iteratively revises its structure while maintaining structural validity; steps 9–10 are omitted as changes from step 8 are negligible. **Claude** demonstrates meaningful visual self-correction: it produces a plausible roof (called: gambrel style) by step 2 but with an incorrect ridge orientation, then progressively corrects across subsequent steps, converging to the almost right form by step 8. **GPT-5** commits to an incorrect orientation from step 1 and fails to recover, instead collapsing into a hybrid that blends both orientations without resolving either. **Gemini** makes minimal modifications across all 10 attempts, suggesting it does not meaningfully incorporate the visual feedback signal. This example illustrates the key behavioral divergence in this experiment: models differ not only in final score, but in *whether* they engage with feedback at all.

O3: Some Models can see structure under the skin, some cannot.

Claude and Gemini improve structurally under Facade input (Claude 71.6% \rightarrow 77.9%; Gemini 45.4% \rightarrow 53.9%); GPT-5 declines sharply (79.2% \rightarrow 63.7%). Gemini is the only model whose visual score also improves (0.376 \rightarrow 0.394), suggesting it activates strong architectural priors when reasoning through appearance to infer under-

lying structure. GPT-5, relying on direct structural mimicry, is disrupted when the framing signal is occluded by cladding.

O4: Protocol dominates model.

The performance gap attributable to protocol choice exceeds any cross-model difference within a fixed protocol. Gemini swings from 45.4% to 78.5% structural pass rate, a 33 points gain, sim-

ply by changing from Planner-Atomic to Planner-Managed. Crucially, Gemini *overtakes* GPT-5 under Planner-Managed despite trailing it by 34 points under Planner-Atomic, a rank reversal impossible to predict from single-protocol evaluation alone. This suggests that agentic scaffold design is at least as consequential as model selection: the same model can be the weakest or the strongest depending on how the task is structured.

Other Observations. Topological proximity does not guarantee structural validity. Composite topological scores are nearly identical between passed and failed structures: in Planner-Atomic, passed vs. failed scores are 0.164 vs. 0.149 (Claude), 0.171 vs. 0.175 (Gemini), 0.143 vs. 0.131 (GPT-5); *see Appendix for details*. For Gemini, failed structures score *higher* topologically than passing ones. Physical constraints are *discontinuous*, a single missed connection or an over-span fails the entire structure with no partial credit while topological and visual metrics are smooth and continuous. Because of this fundamental mismatch, standard perceptual benchmarks cannot be relied upon. They merely measure how accurate a structure *looks* overall, making them insufficient proxies for evaluating whether a model actually understands true physical generative reasoning.

4.2. Iterative Refinement with Visual Feedback

Can iterative visual feedback improve similarity while maintaining structural validity? Starting from Planner-Atomic structural passes with Visual Fidelity $S < 0.6$ (*see Appendix for reason*), we run up to 10 visual-feedback revisions with structural validation enforced at every step. Table 2 reports results.

Structural retention at the final attempt is 68.5% for Claude, 73.8% for Gemini and 78.1% for GPT-5, confirming visual feedback does not catastrophically destabilize structural integrity. Visual scores improvement is moderate but consistent: Claude gains most (+0.033, 70.3% of Tasks improved); Gemini and GPT-5 gain less but still with more than

half of the tasks’ visual score improved.

5. Conclusion

We introduced DreamHouse, a benchmark for *physical generative reasoning* in timber-frame construction. Evaluating four frontier VLMs reveals that structural validity and visual plausibility are orthogonal signals. Models ranking similarly on standard leaderboards diverge sharply here, yielding structural success rates from 15.7% to 79.2% and exhibiting qualitatively distinct failure modes. Crucially, performance is highly sensitive to the generation protocol: a model’s assigned paradigm (holistic vs. stepwise) often impacts correctness more than the choice of model itself. This demonstrates that *how* a model is asked to reason about physical space matters as much as what it inherently knows. These results expose a gap in current evaluations: the ability to maintain global structural consistency, such as load-path continuity and code-compliant spans within complex real-world building systems. We hope DreamHouse and its validation suite serve as a concrete, verifiable target to track progress in this domain.

Limitations and future work. High computational costs for executing validation scripts at scale currently limit our evaluation to closed-source frontier models. Future work should extend our physical constraint vocabulary to encompass concrete, steel, or multi-material assemblies. Furthermore, while we primarily evaluate the *output* generation pipeline, exploring the *input* end is vital, identifying visual representations, supervision signals, or training objectives that enable models to proactively internalize structural grammar rather than merely recovering it through iterative feedback.

Appendix

Appendix provides additional details on the dataset construction, evaluation protocol, model prompts, and extended experimental results that complement the main paper.

6. Structural Validation Suite

6.1. Load Path (Topological Connectivity)

6.1.1. Setup

Let $\mathcal{S} = (V, E)$ be an undirected graph where $V = \{v_1, \dots, v_n\}$ is the set of structural members and E is the adjacency relation. For each member v_i , define its world-space axis-aligned bounding box (AABB):

$$\text{AABB}_i = [x_i^-, x_i^+] \times [y_i^-, y_i^+] \times [z_i^-, z_i^+]$$

Definition 1 (Contact Relation). *Two members $v_i, v_j \in V$ are adjacent, written $v_i \sim v_j$, iff their AABBs overlap with tolerance $\varepsilon = 0.05$ m, i.e. for each axis $k \in \{x, y, z\}$ the true gap satisfies*

$$\delta_k = \max(0, \max(a_k^-, b_k^-) - \min(a_k^+, b_k^+)) \leq \varepsilon.$$

Definition 2 (Ground Set). $G = \{v_i \in V \mid z_i^- < 0.1 \text{ m}\}$.

Definition 3 (Support Function). $\sigma : V \rightarrow \{0, 1\}$ is the fixed point of:

$$\sigma(v_i) = \begin{cases} 1 & v_i \in G \\ 1 & \exists v_j \sim v_i, \sigma(v_j) = 1 \\ 0 & \text{otherwise} \end{cases}$$

computed iteratively until convergence.

6.1.2. Test Criterion

$$T_1 = \text{PASS} \iff \sigma(v_i) = 1 \quad \forall v_i \in V$$

6.2. Span Limits (IRC Compliance)

6.2.1. Setup

For each joist or rafter v_i , let L_i be the clear span, (w_i, d_i) the cross-section dimensions, and $\tau = 0.03$ the span tolerance. IRC look-up tables give allowable spans:

$$\mathcal{T}_J : (w_i, d_i) \mapsto L_J^*, \quad \mathcal{T}_R : (w_i, d_i) \mapsto L_R^*.$$

6.2.2. Effective Span Reduction

When purlins are present, rafter effective span is halved:

$$L_i^{\text{eff}} = \begin{cases} L_i/2 & \text{purlin present} \\ L_i & \text{otherwise} \end{cases}$$

6.2.3. Test Criterion

$$T_2 = \text{PASS} \iff \begin{cases} L_i \leq (1+\tau)L_J^* & \forall v_i \in \text{Joists} \\ L_i^{\text{eff}} \leq (1+\tau)L_R^* & \forall v_i \in \text{Rafters} \end{cases}$$

6.3. On-Centre Spacing (16"/24")

6.3.1. Setup

Group joists sharing the same elevation and direction into sets \mathcal{G}_k . Sort each group by perpendicular position and form the spacing sequence $s_\ell = p_{\ell+1} - p_\ell$. Standard spacings: $\mathcal{S} = \{0.406, 0.610\}$ m.

Definition 4 (Compliant Spacing). s_ℓ is compliant if $\min_{s^* \in \mathcal{S}} |s_\ell - s^*| < 0.05$ m.

6.3.2. Test Criterion

$$T_3 = \text{PASS} \iff \forall \mathcal{G}_k, \ell : s_\ell \text{ compliant} \vee s_\ell \leq 0.1 \text{ m}$$

6.4. Standard Lumber Dimensions

6.4.1. Setup

Let Λ be the standard nominal-dimension set (metric actual sizes, mm):

$$\Lambda = \{(38, 89), (38, 140), (38, 184), (38, 235), (38, 286), (89, 89), (140, 140)\}$$

For each framing member v_i , let $\mathbf{d}_i = (\min(\Delta_i), \text{med}(\Delta_i))$ be its two smallest cross-section dimensions.

6.4.2. Test Criterion

$$T_4 = \text{PASS} \iff \forall v_i \exists (w^*, d^*) \in \Lambda : \begin{aligned} &|d_{i,1} - w^*| < 10 \text{ mm} \\ &\wedge |d_{i,2} - d^*| < 20 \text{ mm} \end{aligned}$$

6.5. Deflection (L/360 Serviceability)

6.5.1. Setup

For each joist v_i : uniform load $w = 1900$ N/m, $E = 12$ GPa, and $I_i = b_i h_i^3 / 12$, where $b_i = \min(\Delta x_i, \Delta y_i)$ and $h_i = \Delta z_i$. Mid-span deflection and limit:

$$\delta_i = \frac{5wL_i^4}{384EI_i}, \quad \delta_i^* = \frac{L_i}{360}.$$

6.5.2. Test Criterion

$$T_5 = \text{PASS} \iff \forall v_i \in \text{Joists} : \delta_i \leq (1 + \tau_\delta) \delta_i^*$$

where $\tau_\delta = 0.08$ (8% deflection tolerance).

6.6. Roof Coverage

6.6.1. Setup

Partition the footprint into $1 \text{ m} \times 1 \text{ m}$ cells. Let \mathcal{F} be cells occupied by floor/sill objects, and $\mathcal{R} \subseteq \mathcal{F}$ cells covered by at least one rafter projection (margin $\mu = 0.3$ m). Coverage ratio:

$$\rho = |\mathcal{R}| / |\mathcal{F}|.$$

6.6.2. Test Criterion

$$T_6 = \text{PASS} \iff \rho \geq 0.70$$

6.7. Gap Detection

6.7.1. Setup

Using the grid from Test 6, the gap set is $\mathcal{Q} = \mathcal{F} \setminus \mathcal{R}$ and the gap ratio $\gamma = |\mathcal{Q}| / |\mathcal{F}|$.

6.7.2. Test Criterion

$$T_7 = \text{PASS} \iff \gamma \leq 0.20$$

Since $\rho + \gamma = 1$, T_7 is equivalent to T_6 at the same threshold; both are retained for diagnostic granularity.

6.8. Cantilever Limits

6.8.1. Setup

Let \mathcal{P} be ground-reaching supports ($z_i^- < 0.1$ m). For each elevated sill s ($z_s^- > 1.0$ m), let ℓ_s be its length and \mathcal{P}_s the nearby supports (within $c_{\max} = 1.5$ m laterally). For long sills ($\ell_s > c_{\text{sp}} = 3.0$ m), let Δ_s^{\max} be the maximum gap between consecutive supports along the sill axis.

6.8.2. Test Criterion

$$T_8 = \text{PASS} \iff \forall s \in \text{ElevSills} : \begin{cases} |\mathcal{P}_s| \geq 2 \wedge \Delta_s^{\max} \leq c_{\text{sp}} & \ell_s > c_{\text{sp}} \\ d(s, \mathcal{P}_s) \leq c_{\max} & \text{otherwise} \end{cases}$$

6.9. Stability Score

6.9.1. Definition

The *Topological Stability Index* (TSI) is:

$$\Sigma = \frac{\sum_{v_i \in V} \sigma(v_i)}{|V|}$$

6.9.2. Test Criterion

$$T_9 = \text{PASS} \iff \Sigma \geq 1.0$$

$\Sigma = 1.0$ means every member's load path terminates at a grounded element. T_9 is strictly stronger than T_1 : T_1 checks binary grounding; T_9 requires the full set V to be grounded simultaneously.

6.10. Dual-End Connection

6.10.1. Setup

For each rafter or stud v_i with height $h_i = z_i^+ - z_i^- \geq 0.3$ m, define connection zones:

$$Z_i^{\text{bot}} = [z_i^-, z_i^- + \alpha h_i], \quad Z_i^{\text{top}} = [z_i^+ - \alpha h_i, z_i^+]$$

where $\alpha = 0.20$.

Definition 5 (Zone Connection). v_j connects to zone Z_i^{bot} (resp. Z_i^{top}) of v_i if: (i) v_j overlaps v_i in xy with tolerance $\varepsilon_c = 0.10$ m, and (ii) $[z_j^-, z_j^+]$ intersects that zone with tolerance ε_c .

Let $\phi_i^{\text{bot}}, \phi_i^{\text{top}} \in \{0, 1\}$ indicate bottom/top zone connections.

6.10.2. Test Criterion

$$T_{10} = \text{PASS} \iff \forall v_i \in \text{Rafters} \cup \text{Studs} : \phi_i^{\text{bot}} = 1 \wedge \phi_i^{\text{top}} = 1$$

A rafter missing its top connection (ridge/collar) has a free end and may rotate under load (*hinge failure*). A stud missing its bottom connection (sole plate) is a *floating column*.

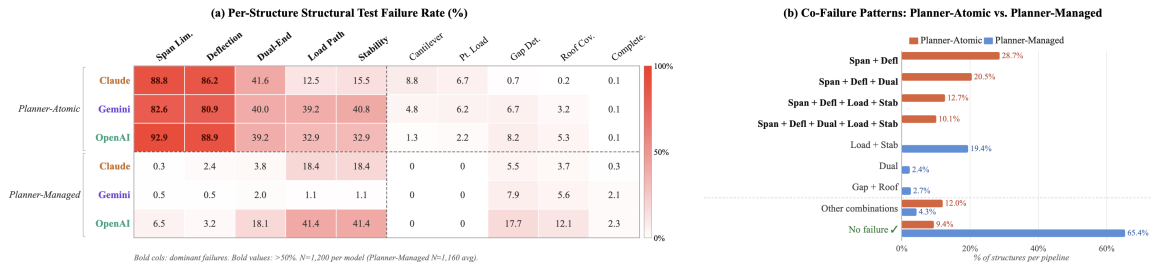


Figure 7. **Structural failure analysis across pipelines and models.** (a) Per-structure failure rate for each of the 10 structural validation tests, shown for the Planner-Atomic and Planner-Managed protocols across all three models ($N = 1,200$ per model for Planner-Atomic; $N \approx 1,160-1,197$ for Planner-Managed, excluding Phase-0 failures). Each cell reports the percentage of structures for which that test failed at least once across all retry attempts. Values are independent marginal failure rates per test and do not sum to 100% per row, as a single structure can fail multiple tests simultaneously. Bold column headers indicate the five dominant failure tests. (b) Co-failure pattern distribution: each structure is assigned to the exact set of tests it failed, ranked by frequency. Orange bars show Planner-Atomic ($N = 3,551$); blue bars show Planner-Managed ($N = 3,484$), each normalized to their respective totals. The top four Planner-Atomic patterns share a Span + Deflection core, reflecting near-universal geometry violations. Planner-Managed failures are dominated by Load + Stability errors, indicating structural connectivity issues rather than geometric ones.

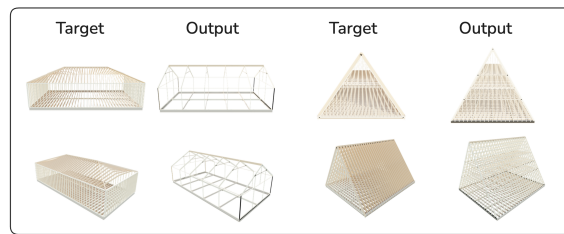


Figure 8. **Typical failure modes of Claude 4.5 opus (Planner-Reactive).** Each pair shows a ground-truth target structure (left) alongside Claude's generated output (right) for configurations RN_01_0035 (left pair) and AF_05_0713 (right pair). Claude's outputs exhibit two characteristic failure patterns: RN_01_0035 produces an overly sparse frame with missing members, while AF_05_0713 produces an overly dense packing of repeated elements. Both reflect insufficient adherence to IRC structural rules, the model optimizes for visual plausibility rather than code-compliant member placement, resulting in structures that fail span limit and deflection validation despite appearing superficially similar to the target geometry.

Summary Table

6.11. Level of Detail 350 and the Dream-House Validation Standard

What LoD 350 Requires. The BIM Forum's Level of Development specification defines *Level of Detail 350* (LoD 350) as the threshold at which a model element is sufficiently detailed for *construction coordination* [10]. Concretely, LoD 350 requires that every structural member be modeled with:

- (i) **Accurate geometry** — cross-section dimensions matching nominal fabrication tolerances (≤ 3 mm deviation from specification);
- (ii) **Correct spatial position** — no hard clashes, defined as two members occupying the same physical volume with overlap exceeding construction tolerance;
- (iii) **Interface definition** — each member must explicitly represent the connections and clearances needed by adjacent trades (e.g.

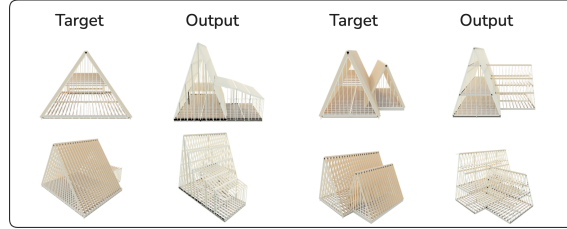


Figure 9. **Representative failure modes of Gemini-3-flash on A-frame structures under the Planner-Reactive protocol.** Each pair shows the target structure (left) and the model output (right). Left pair AF_03_0392: Gemini correctly identifies the A-frame geometry and rafter count but misplaces the side wing, attaching it to the wrong elevation face and inverting the attachment axis, producing a structure that passes visual inspection from one view but fails load-path and dual-end connection tests. Right pair AF_04_0460: The ridge direction is rotated 90° relative to the target, causing all rafters to span the wrong axis; the resulting assembly passes geometric tests (T_3 , T_4) but fails roof coverage (T_6) and gap detection (T_7) entirely. These errors illustrate a systematic failure mode: Gemini recovers *what* structural elements are present but not *where* they are oriented, consistent with $O3$: the model attends to member topology but not to the 3-D spatial relationships encoded in the multi-view input.

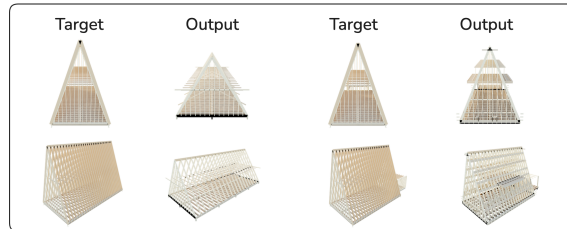


Figure 10. **Representative failure modes of GPT-5 on A-frame structures under the Planner-Reactive protocol.** Each pair shows the target structure (left) and the model output (right). Left pair AF_02_0182: GPT-5 reproduces the correct rafter count and overall A-frame silhouette but generates collar ties and floor joists that extend beyond the structure’s bounding envelope, with members protruding outside the intended footprint. The assembly fails dual-end connection (T_{10}) and gap detection (T_7) as a result. Right pair AF_03_0318: A similar pattern: the rafter and joist layout is topologically correct but spatially unconstrained, members overshoot the ridge and sill attachment zones, leaving floating ends unconnected to the load path. Both failures share a common root cause: GPT-5 reasons about *which* members to place but not about the spatial envelope that bounds them, treating member generation as an independent local decision rather than a globally constrained packing problem. This geometric incapability, the inability to enforce that every member end terminates within a valid connection zone, is the dominant failure signature of GPT-5 across A-frame styles and is consistent with $O2$: structural reasoning is not monolithic, and spatial constraint satisfaction is a capability that does not co-occur with topological correctness.

- (iv) **Load-path integrity** — the assembly must support a credible load transfer hierarchy from applied loads to the foundation without floating or unsupported members.

Below LoD 350 (i.e. LoD 200–300), members may be represented as “placeholders” with approximate

geometry; above it (LoD 400), full fabrication detailing is included. LoD 350 is therefore the *minimum standard for constructibility review* and the natural target for automated structural generation.

Mapping LoD 350 to Our 10-Test Battery. Each requirement above maps directly to one or

Test	Name	Pass Condition	Category
T_1	Load Path	$\sigma(v_i) = 1 \forall i$	IRC / Structural
T_2	Span Limits	$L_i^{\text{eff}} \leq (1 + \tau)L^*$	IRC / Structural
T_3	O.C. Spacing	$s_\ell \in \mathcal{S} \pm 0.05 \text{ m}$	IRC / Geometric
T_4	Std. Dimensions	$(w_i, d_i) \in \Lambda$	Geometric
T_5	Deflection L/360	$\delta_i \leq (1 + \tau_\delta)L_i/360$	Physics
T_6	Roof Coverage	$\rho \geq 0.70$	Geometric
T_7	Gap Detection	$\gamma \leq 0.20$	Geometric
T_8	Cantilever Limits	Support spacing $\leq 3.0 \text{ m}$	Structural
T_9	Stability Score	$\Sigma = 1.0$	Topological
T_{10}	Dual-End Connection	$\phi_i^{\text{bot}} = \phi_i^{\text{top}} = 1 \forall i$	Structural

more tests in our validation suite (Table 3). Requirement (i) corresponds to T_4 (standard lumber dimensions) and T_2 (span limits, which implicitly enforce cross-section adequacy). Requirement (ii) is addressed by T_7 (gap detection) and the clash detection module embedded in T_9 . Requirement (iii) is enforced by T_{10} (dual-end connection), which checks that every rafter and stud is restrained at both ends, the minimum condition for a mechanically complete interface. Requirement (iv) is captured most directly by T_1 (load path) and T_9 (Topological Stability Index), with T_8 (cantilever limits) addressing the specific case of elevated sections that satisfy local connectivity but violate global load-path continuity.

Why LoD 350 Is the Right Target for Physical Generative Reasoning. Prior work on AI-assisted architectural generation has largely operated at LoD 100–200, producing massing models or schematic floor plans that are *visually plausible* but not *physically constructible* [30, 36]. We argue that this constitutes a fundamental gap: a model that cannot satisfy LoD 350 constraints cannot reason about the physical world, only about its appearance. DreamHouse is specifically designed to close this gap. By grounding evaluation in LoD 350 criteria and operationalizing those criteria as formal, executable tests. We provide a benchmark at which the distinction between *perceptual generation* and *physical generation* becomes measurable.

Concretely, passing all ten tests in our suite is a

necessary (though not sufficient) condition for LoD 350 compliance in timber-frame residential construction. Sufficiency would additionally require fastener schedules, bearing plate sizing, and anchor bolt layouts (LoD 400 territory); we treat these as out of scope for the current benchmark but note them as a natural extension.

7. Visual Similarity Metric and Score Choice

We describe the full derivation of the visual similarity score S , justify the choice of alpha-weighted MSE over perceptual alternatives, and detail the view configuration used across all experiments.

7.1. Score Derivation and Threshold Selection

7.1.1. Alpha-Weighted MSE Formulation.

Let $\hat{R}_v \in [0, 1]^{H \times W \times 3}$ be a rendered RGB image of a VLM-generated structure and $R_v \in [0, 1]^{H \times W \times 3}$ be the corresponding reference render of the ground-truth structure, both produced from the same viewpoint v . Let $m_v = \alpha_v^g \cup \alpha_v^r$ be the union alpha mask of the generated and reference renders, restricting comparison to non-transparent regions of either structure. The *alpha-weighted mean squared error* is:

Table 3. Mapping of LoD 350 constructibility requirements to the DreamHouse validation tests.

LoD 350 Requirement	Tests	What Failure Means
(i) Accurate geometry	T_4, T_2, T_5	Non-standard cross-sections; spans exceeding IRC limits; serviceability failure under design load
(ii) No hard clashes	T_7, T_3	Members overlap or leave gaps wider than one stud bay; framing cannot be physically assembled
(iii) Interface definition	T_{10}, T_6	Rafters/studs free at one end (hinge failure under load); roof plane incompletely framed
(iv) Load-path integrity	T_1, T_9, T_8	Floating members; unsupported elevated sections; Topological Stability Index < 1.0

$$\text{MSE}_v = \frac{\sum_p m_v(p) \cdot \|\hat{R}_v(p) - R_v(p)\|^2}{\sum_p m_v(p)}$$

where p indexes spatial pixels and the denominator normalises by the foreground area. The union mask penalizes missing geometry: a member absent in the generated structure leaves unmatched non-transparent pixels in the target without rewarding empty background agreement.

7.1.2. Per-View Score.

The raw MSE is mapped to a bounded similarity score via a linear transformation calibrated so that $\text{MSE}_v = 0$ gives $S_v = 1.0$ (perfect match) and $\text{MSE}_v = 0.1$ gives $S_v = 0.0$ (total failure):

$$S_v = \max(0, 1 - \lambda \cdot \text{MSE}_v)$$

where $\lambda = 10$. The linear form is intentional: it avoids the saturation behaviour of sigmoid-based mappings that would compress differences in the high-quality regime ($S_v > 0.8$) where our benchmark discriminates most finely between models. The aggregate visual similarity score reported in all tables is:

$$S = \frac{1}{V} \sum_{v=1}^V S_v$$

averaged over $V = 5$ views, consistent with Eq. (1) of the main paper.

7.1.3. Joint Pass Condition Across Five Views.

A single-view score is insufficient because a structure may appear correct from the front while having a collapsed rear wall or missing roof section. We therefore require the score to exceed threshold τ on *all* five views simultaneously. Let S_v denote the per-view score for view $v \in \{1, \dots, 5\}$. The binary *visual pass* indicator is:

$$\mathbb{K}_{\text{vis}} = \prod_{v=1}^5 \mathbf{1}[S_v \geq \tau]$$

7.1.4. Threshold Selection: $\tau = 0.6$.

The joint pass condition is strict by design: a structure must exceed τ on *every* view simultaneously. We set $\tau = 0.6$ as the lowest threshold at which the joint pass rate remains non-trivially above zero across all models. Lower values admit structures with obvious structural failures while providing no discriminative signal, and the joint condition at any higher threshold collapses all models to near-zero pass rates. The $\tau = 0.6$ operating point thus represents the most demanding threshold that keeps the benchmark informative across all evaluated models.

Table 4. Camera configuration for the five views. c_v is the distance multiplier.

View	Azimuth	Elevation	c_v
Front	0°	12°	1.05
Back	180°	12°	1.05
Left	270°	12°	1.05
Right	90°	12°	1.05
Front-right	45°	18°	1.10

7.2. Orthographic View Configuration

7.2.1. View Definitions.

All renders use *perspective projection* (focal length 32 mm) with camera distance scaled to the structure’s bounding diagonal. The five canonical views are:

7.2.2. Rationale for View Selection.

The five views were chosen to provide *complementary coverage* of the structure such that no single structural failure mode is invisible across all views:

- **Views 1–4** (cardinal elevations) detect wall misalignment, wrong storey height, missing or misplaced openings, and incorrect roof pitch.
- **View 5** (front-right isometric) reveals three-dimensional failures: depth errors, missing rear framing, and roof asymmetries that are ambiguous in any single cardinal view.

7.2.3. Distance Normalisation.

For each view v , the camera is placed at distance

$$d_v = c_v \cdot D$$

where $D = \|\mathbf{p}_{\max} - \mathbf{p}_{\min}\|_2$ is the world-space bounding diagonal of the structure and c_v is the per-view multiplier (Table 4). The camera always points at the structure’s bounding-box centroid $\mathbf{b} = (\mathbf{p}_{\max} + \mathbf{p}_{\min})/2$.

Scaling by D ensures that structures of different sizes, from 7 m × 7 m cottages to 14 m × 14 m two-storey colonials, always fill the frame comparably, without requiring a hard-coded minimum distance. Both the generated and reference renders use identical camera parameters derived from their respec-

tive bounding diagonals, so any residual scale difference is absorbed by the fixed 512 × 512 resize applied before MSE computation.

8. Bridge Benchmark: Motivating Example

Prior to settling on timber-frame construction as the testbed for DreamHouse, we piloted a **bridge-generation** benchmark as an alternative domain for physical generative reasoning. The task asked frontier VLMs to generate a structurally valid truss or arch bridge given a reference render, outputting a `BridgeParams` dataclass that was then validated against a 26-test suite (AASHTO LRFD [7], AISC 360 [8], ACI 318 [4]) and re-rendered for visual comparison. On the surface, the domain appeared well-suited: the validation criteria are formally codified, the geometry is spatially unambiguous, and the renders are visually rich.

The Shortcut. We observed that frontier VLMs could recover a near-perfect `BridgeParams` dict from a single reference image *in one shot*, requiring no iterative refinement. The outputs passed all validation tests and were visually indistinguishable from the ground-truth renders. Closer inspection revealed why: the render pipeline exposes a *low-dimensional, analytically invertible* parametric space.

Concretely, the render script (`bridge_render.py`) places the camera at a fixed distance $d = c \cdot L$ proportional to `span_length` L , always pointed at the centroid of the bounding box. The truss geometry is then a deterministic function of six scalar parameters: `span_length`, `truss_height`, `num_panels`, `deck_width`, `chord_width`, and `arch_rise`, each of which projects to a directly measurable visual quantity in the render: apparent span-to-height ratio, panel count (a discrete integer legible from the image), deck-to-span width ratio, and so on. Furthermore, the validation tests themselves impose *tight algebraic constraints* that further reduce degrees of freedom: the span/depth ratio must lie in [7, 11] (Test 1), the

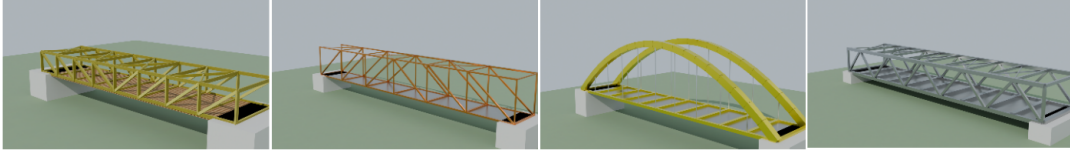


Figure 11. Representative renders from the bridge generation pilot: glulam Howe truss (left), steel Pratt truss (center-left), steel arch (center-right), and steel Warren truss (right). Each bridge is fully parameterized by a low-dimensional `BridgeParams` dataclass whose scalar fields: `span_length`, `truss_height`, `num_panels`, `deck_width` project directly to measurable visual quantities in the render. Frontier VLMs recovered valid parameters from a single reference image in one shot with no iterative refinement, exposing the domain as a visual measurement task rather than a test of structural reasoning. This failure mode motivated the shift to timber-frame construction, where the structurally critical quantities are interior to the assembly and not directly legible from exterior renders.

panel aspect ratio in $[0.65, 1.40]$ (Test 6), the arch rise ratio in $[0.10, 0.40]$ (Test 7). A model that can read two distances from an image and solve a pair of inequalities can satisfy these tests without any structural understanding.

In short, the bridge benchmark collapsed into a *visual measurement task*: estimate a handful of lengths from the image, verify they satisfy publicly available code ratios, and instantiate the dataclass. No reasoning about member connectivity, load path topology, or construction hierarchy was required.

Why Timber Framing Forecloses This Shortcut. Timber-frame residential construction lacks a low-dimensional parametric representation that is directly legible from exterior renders. The structurally critical quantities in DreamHouse: member spacing, connection zone assignment, load-path topology ($\sigma(v_i) = 1 \forall i$), dual-end restraint, and IRC span compliance are *interior properties* of the framing assembly that are partially or wholly occluded in any single render. A wall shifted 0.5 m or a joist missing its end connection looks nearly identical from the outside but fails multiple validation tests. No analytic inversion of the render exists because the mapping from framing topology to exterior appearance is many-to-one and non-injective: different assemblies produce indistinguishable renders while differing in load path, cantilever adequacy, and structural stability.

This is the key asymmetry between the two domains. Bridge geometry is *exoskeletal* the struc-

tural members are the exterior, so visual similarity and structural correctness are tightly coupled. Timber framing is *endoskeletal*, the structure is concealed behind cladding so the two are largely decoupled. DreamHouse is specifically designed to exploit this decoupling: a model cannot achieve high structural pass rates by visual pattern matching alone, and the 7.1% joint pass rate observed across all frontier models (main paper, Table 2) confirms that the shortcut available in the bridge domain is not available here.

9. Extended Experimental Results

9.1. Stepwise with Per-Step Visual Feedback

We evaluated a variant of Planner-Managed in which the rendered output is compared against the target after each construction step and visual similarity feedback is appended to the prompt before the next step. Table 5 reports structural pass rate, mean visual fidelity, and joint pass rate: the fraction of structures that simultaneously pass all structural tests *and* achieve $S \geq 0.6$ for both conditions.

Joint pass rate. Visual feedback more than doubles the joint pass rate for Claude (+205%, 3.08% \rightarrow 9.40%) and Gemini (+105%, 4.34% \rightarrow 8.90%), while GPT-5 shows only a marginal improvement (+23%, 0.75% \rightarrow 0.92%). The joint metric is the most demanding criterion in our evaluation. It requires the output to be simultaneously safe and visually faithful and the large gains for Claude and Gemini indicate that per-step vi-

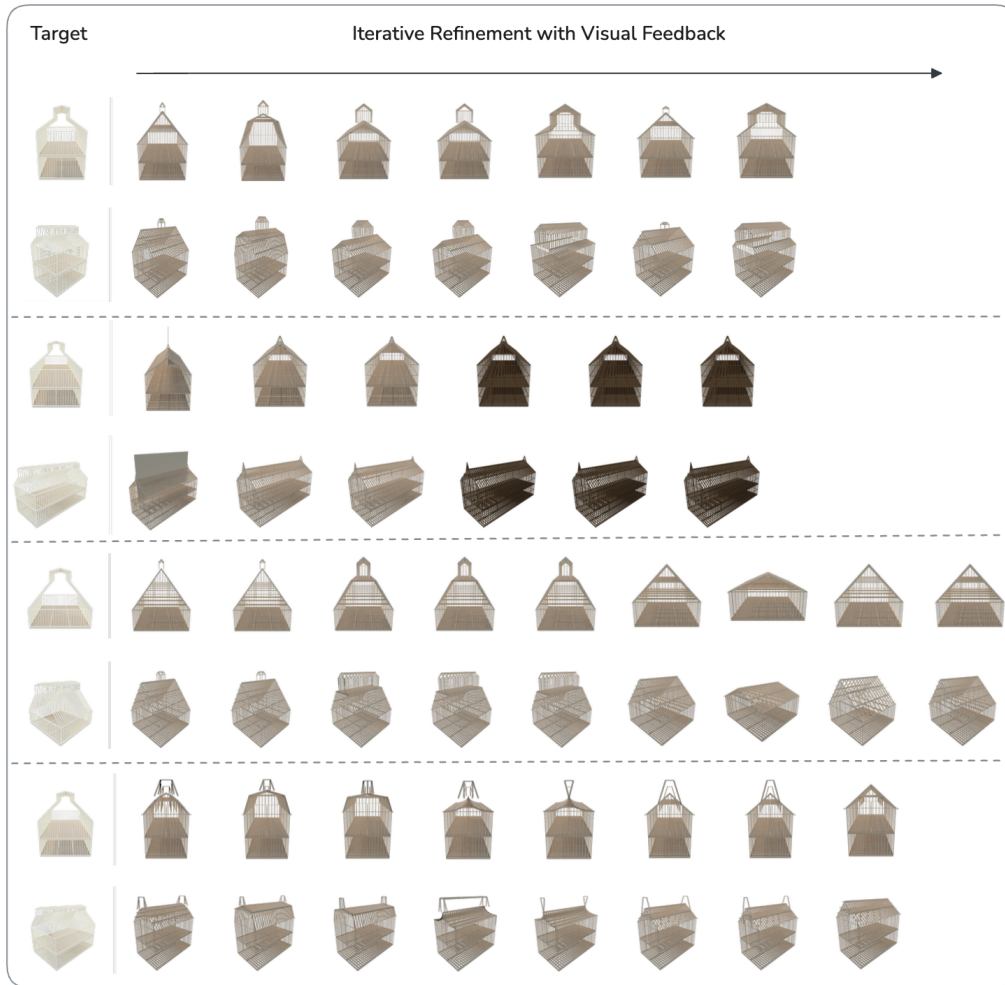


Figure 12. Iterative Refinement with Visual Feedback trajectories for Claude 4.5 opus on four similar barn-style structures. Each pair of rows shows the target (leftmost, lighter color) followed by successive iterations (left to right, darker). Dashed horizontal lines separate groups of structurally distinct targets. Within each group, targets share the same architectural style and similar proportions, yet Claude consistently pursues *different* refinement strategies across instances: some trajectories make large structural revisions between iterations (roof skeleton replaced); others converge quickly and make only minor adjustments; others oscillate without monotonic improvement. This variability within a homogeneous style group reveals that Claude’s behavior is not driven by a stable visual error signal, it does not reliably identify the same class of discrepancy across similar targets and apply a consistent corrective action. Rather, each iteration represents an independent re-interpretation of the feedback, which can move the output toward or away from the target depending on which aspect of the render the model attends to. This is consistent with $O1$ and $O3$: visual similarity and structural validity are orthogonal, and the ability to *see* a structural error in a rendered image does not imply the ability to *correct* it in the next generation.

sual grounding helps models resolve the orthogonality between structural validity and visual simi-

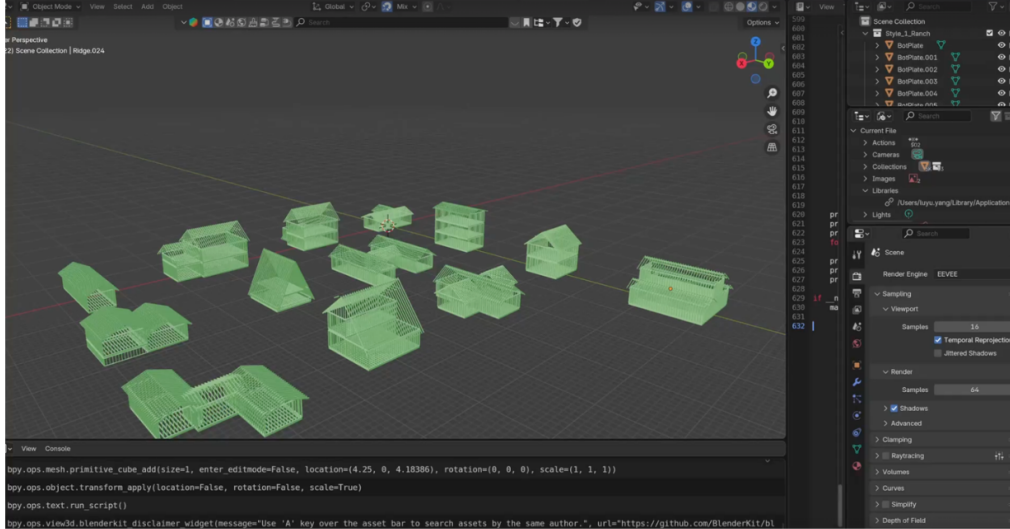


Figure 13. The 13 architectural style archetypes visualized in Blender, shown as wireframe meshes in the 3D viewport. Each archetype defines the canonical massing, roof type, section layout, and story count for one style category in the DreamHouse dataset. The procedural generation pipeline instantiates each archetype across a range of lot sizes, proportions, and complexity levels to produce the 26,000+ structure dataset. Structures are rendered headless via the Blender Python API (`bpy`); the console output visible at the bottom shows a representative member placement call during procedural construction.

larity identified in O1.

Structural vs. visual trade-off. The two objectives do not always improve together under visual feedback. Claude gains on both axes: structural pass rate increases by +6.67 percentage points and Visual Fidelity increases by +3.7%. Gemini, however, trades a small structural regression (−4.45 pp) for a large visual gain: the fraction of structures passing $S \geq 0.6$ nearly triples (5.4% → 13.3%). GPT-5 declines slightly on both axes, suggesting that visual feedback does not compensate for its underlying spatial constraint failures identified in Figure 10.

Threshold crossing. The most obvious effect of visual feedback is at the $S \geq 0.6$ threshold: all three models show larger relative gains in visual pass rate than in Visual Fidelity, indicating that feedback helps a meaningful subset of structures cross the quality threshold even when the overall mean shifts little. This is consistent with visual feedback acting as a targeted correction signal rather than a uniform

quality lift.

9.2. Open-Source Model Evaluation

We evaluated three open-source models under the Planner-Managed protocol to assess whether the capability gap observed between frontier models extends to publicly available weights.

Qwen3-VL-8B-Instruct and Qwen3-VL-30B-A3B-Instruct. Both models achieved a structural pass rate of 0% across all 10 validation tests under Planner-Managed. Neither model produced syntactically valid Blender Python code reliably enough to complete construction, and when code did execute, the resulting assemblies failed every structural test. We did not collect visual similarity scores for these models as the structures were not renderable.

Kimi K2.5. We additionally ran a small pilot evaluation of Kimi K2.5 under Planner-Managed on a random subset of structures and observed

Table 5. Stepwise (Planner-Managed) **without** per-step visual feedback vs. **with** in *Frame* (timber framing as input). Joint pass rate is the primary metric: structures that are both structurally valid and visually similar ($S \geq 0.6$).

Model	Protocol	Struct. Pass	Visual Fidelity	Visual Pass (≥ 0.6)	Joint Pass
GPT-5	Planner-Managed	0.333	0.179	0.022	0.008
	+ visual feedback	0.317	0.173	0.030	0.009
Claude	Planner-Managed	0.713	0.278	0.043	0.031
	+ visual feedback	0.780	0.288	0.122	0.094
Gemini	Planner-Managed	0.785	0.313	0.054	0.043
	+ visual feedback	0.740	0.311	0.133	0.089

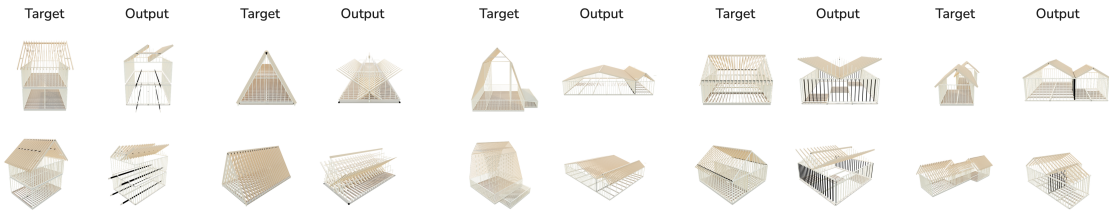


Figure 14. Representative outputs of Qwen3.5-397B-A17B under Planner-Managed, showing five target–output pairs across two views (front elevation, top; diagonal, bottom). Failures are more fundamental than those observed in frontier models: **columns 1, 2, 4** show incorrect rafter orientation — rafters span the wrong axis entirely, producing a roof that is geometrically inverted relative to the target; **column 3** exhibits severe global disproportion, with the generated structure roughly half the height and twice the footprint of the target, indicating a failure to infer absolute scale from the multi-view input; **column 5** shows a collapsed depth dimension, the 3D volume is flattened into a near-planar assembly that passes a front-view silhouette check but has no structural depth. Unlike the frontier model failures in Figures 8 and 9, which involve spatially misplaced but topologically coherent members, Qwen3.5 errors reflect a lack of basic 3D spatial grounding, the model does not reliably recover the orientation, scale, or depth of the target structure from the provided views.

a structural pass rate of 0%, consistent with the Qwen3-VL results. Given that three independent open-source model families: spanning dense and sparse MoE architectures, and parameter counts from 8B to 397B all failed to produce analyzable structural outputs, we discontinued the open-source evaluation track. The benchmark in its current form requires code generation and spatial reasoning capabilities that appear to be frontier-only, and we leave open-source model improvement as future work.

Qwen3.5-397B-A17B. We subsequently evaluated Qwen3.5-397B-A17B [3], a sparse mixture-

of-experts model with 17B active parameters, accessed via the Novita AI OpenAI-compatible endpoint under the same Planner-Managed hyperparameters used for frontier models (5 retries per step, 30 global retries, 5-step history truncation, $\tau_{\text{retry}} = 0.4$). Visual similarity checks were disabled for this run (`require_visual_similarity: false`) as the model’s code reliability was uncertain.

Out of 1,200 structures, 247 (20.6%) produced renderable outputs. The structural pass rate on this subset was 20.6%. Mean visual similarity was $\bar{S} = 0.261$ (median 0.220), well below all frontier models. Per-view scores were lowest for the back view ($S_2 = 0.167$) and highest for the front-right

diagonal ($S_5 = 0.418$), consistent with the model producing a plausible front silhouette while failing to close the rear framing. Joint visual pass rates collapsed rapidly with threshold: 15.4% at $S \geq 0.3$, 10.1% at $S \geq 0.4$, and 1.6% at $S \geq 0.6$.

These results confirm that the DreamHouse tasks remain out-of-reach for current open-source models even at the 397B scale, and that the benchmark discriminates meaningfully between frontier and non-frontier capability levels. The 79.4% non-renderable rate for Qwen3.5 versus near-zero for GPT-5, Claude, and Gemini, further highlights that reliable Blender Python code generation is itself a frontier capability.

9.3. Structural Error Map Visualizations

Figure 7 provides a fine-grained breakdown of *where* models fail structurally, complementing the aggregate pass rates reported in the main paper. Panel (a) reports per-test marginal failure rates across the three protocols (Planner-Atomic, Planner-Reactive) and Planner-Managed; panel (b) shows the distribution of co-failure patterns, the exact sets of tests that fail together on the same structure.

Dominant failure modes differ by protocol (O4).

Under Planner-Atomic protocols, failures are concentrated in the geometry cluster: Span Limits (T_2), Deflection (T_5), and O.C. Spacing (T_3) account for the majority of per-test failures, and the top co-failure patterns in panel (b) all share a Span+Deflection core. This reflects a systematic tendency to generate members with plausible proportions but incorrect absolute dimensions, the structure *looks* right but fails quantitative IRC limits. Under Stepwise, the failure profile shifts sharply toward the connectivity cluster: Load Path (T_1) and Stability Score (T_9) dominate, with co-failure patterns driven by Load+Stability errors. This is consistent with O4 (protocol dominates model): the stepwise interface decomposes the task into member-by-member decisions that accumulate connectivity errors even when individual members are geometrically well-formed.

Structural reasoning is not monolithic (O2).

The per-test failure rates in panel (a) reveal that no model fails uniformly across all tests. Models that perform well on geometric tests (T_3, T_4) frequently fail load-path tests (T_1, T_9), and vice versa. This decomposition supports O2: structural competence is multi-dimensional, and a model’s overall pass rate conflates distinct capabilities: dimensional reasoning, topological connectivity, and IRC code compliance that need not co-occur. The five dominant failure tests (bold column headers in panel (a)) account for the large majority of all failures, suggesting that targeted improvement on a small subset of structural skills would disproportionately raise the joint pass rate.

Visual fidelity does not predict structural validity (O1).

The co-failure patterns in panel (b) reveal that many structures with high visual similarity scores S nevertheless fail multiple structural tests simultaneously. The Span+Deflection co-failure pattern, the most common under Planner-Atomic produces renders that are visually near-identical to the ground truth (correct proportions, correct topology) while failing quantitative structural criteria. This is the empirical basis for O1: visual similarity and structural validity are orthogonal axes, and a benchmark that evaluates only S would misclassify the majority of these failures as successes.

Some models see structure under the skin (O3).

Across both panels, Gemini shows a distinctively lower rate of Load Path (T_1) and Stability (T_9) failures relative to GPT-5 and Claude under the Stepwise protocol, even though its geometric failure rates are comparable. This asymmetry, connectivity competence without geometric precision, underlies O3: it is better at maintaining grounded load paths member-by-member, even when individual member dimensions are imprecise.

9.4. Additional Qualitative Results

Figures 8, 9 and 10, show representative one-shot failures for Claude 4.5 opus, Gemini-3-flash and GPT-5 respectively.

Figure 12 shows iterative refinement with visual feedback trajectories for Claude 4.5 opus across four similar barn-style structures, illustrating the high iteration-to-iteration variance in refinement strategy even within a homogeneous style group.

10. Full Prompt Examples

10.1. Prompt 0: Initial Generation Prompt

Prompt 0 is the system-level instruction injected at the start of every Planner-Atomic and Planner-Managed pipeline call. It specifies the task, the Blender coordinate system, the structural member taxonomy, construction dependency rules, and the output JSON schema. The prompt is identical across all three models; only the five rendered view images and four scalar context fields (`lot_size`, `stories`, `roof_type`, `complexity`) are injected per sample. We present the prompt in four parts.

Part 1: Task Definition and Building Context.

The opening section states the task and injects per-sample metadata. The model is asked to produce a structured JSON construction plan from five rendered views. Lot size, story count, roof type, and complexity are injected verbatim from the ground-truth record and must appear exactly in the model's output (the validator rejects plans whose `lot_size` fields do not match to two decimal places).

Prompt 0 — Part 1:
Task Definition and Building Context

```
# Timber Frame Construction
Planning

## Your Task
Create a detailed construction plan
for the timber frame structure
shown in the images. Your plan
must specify:
1. Section decomposition
2. Construction phases (foundation
-> floor -> walls -> roof)
3. Step-by-step build order with
dependencies
4. Classification of each step as
```

```
"safe" or "critical"
5. Member types and approximate
counts for each step

## Building Context [injected per
sample]
- Lot Size: {width}m x {depth}m
(area: {area}m^2)
CRITICAL: Use EXACT values. Do NOT
recalculate area.
- Stories: {N}
- Roof Type:
{gable|hip|gambrel|shed}
- Complexity:
{simple|moderate|complex}

## Images Provided (5 views, in
this exact order)
Image 1: FRONT VIEW
Image 2: BACK VIEW
Image 3: LEFT VIEW
Image 4: RIGHT VIEW
Image 5: FRONT_RIGHT VIEW
(diagonal)
```

Part 2: Coordinate System and View Definitions.

The second section specifies the Blender world coordinate system and provides a per-view camera table so that the model can correctly interpret left/right/front/back directions when reading pixel-space measurements from each image. This is necessary because the back and right views are mirrored relative to the front view along the x -axis.

Prompt 0 — Part 2:
Coordinate System and View Definitions

```
## Blender Coordinate System

+Z = up, +X = right, +Y =
forward/front

Axis mapping per view:
- front : camera from -Y. X =
left-right, Z = up-down
- back : camera from +Y. X =
right-left (mirrored), Z = up-down
- left : camera from +X. Y =
front-back, Z = up-down
- right : camera from -X. Y =
back-front (mirrored), Z = up-down
```

```

Section bounds use:
- x_min/x_max : left-right extent
- y_min/y_max : front-back extent
(negative Y = back)
- z_base      : ground level
(typically 0.0)

```

```

## How to Analyse Images
Step 1 (Front): count roof peaks,
note step-backs, measure widths.
Step 2 (Sides): confirm depth,
check height differences.
Step 3 (Diagonal): verify 3-D
section relationships.
Step 4: cross-reference all views;
use lot size as sanity check.

```

```

Common section patterns:
- Main body only : rectangular
footprint, one roof
- Main + side wing: L-shaped
- Main + rear wing: T-shaped
- Split-level    : sections at
different z_base values

```

Part 3: Member Taxonomy and Naming Convention. The third section defines the complete set of valid member types, grouped by construction phase, together with the naming convention enforced by the validator. Any member whose name does not begin with one of the listed prefixes (case-sensitive) causes a validation failure and triggers a feedback loop. This section also states the canonical phase dependency chain (foundation → floor → walls → roof) and provides typical spacing and dimension guidelines.

Prompt 0 — Part 3:
Member Taxonomy and Naming Convention

```

## Structural Systems (build in
this order)

Foundation : Sill, BeamPost, Post
Floor      : Rim, Joist,
CenterBeam
Walls     : SolePlate, TopPlate,
Stud, GableStud,
Header, King, Trimmer, Cripple
Roof      : Ridge, Rafter,
Collar, Lookout, Purlin

```

```

CRITICAL naming rule: member names
must START WITH the prefix
(case-sensitive). Valid:
"Sill_front", "Joist_floor1_001"
Invalid: "beam_001",
"vertical_member", "roof_piece"

```

```

Phase dependencies:
- Foundation complete before floor
- Floor complete before walls
- Walls complete before roof
- Multi-story: each story needs
its own floor system
Story 1 floor at z = 0.3m, Story 2
at z = 3.0m, Story 3 at z = 5.7m

```

```

Typical dimensions (guidelines,
not strict):
- Stud spacing   : 0.4m (16") on
centre
- Joist spacing  : 0.4m on centre
- Rafter spacing : 0.6m on centre
- Story height   : 2.7m
floor-to-floor

```

```

Step classification:
CRITICAL: phase transitions, new
sections, elevated construction
SAFE     : adding parallel members
(more joists, more studs)

```

Part 4: Output JSON Schema. The final section specifies the exact JSON schema the model must produce. The validator parses this output and checks: (i) that `lot_size` fields match the injected values exactly; (ii) that all member-type strings match the taxonomy in Part 3; (iii) that `depends_on` indices form a valid directed acyclic graph (DAG) with no cycles; and (iv) that section bounds are consistent with the declared `lot_size`. A condensed excerpt of the schema is shown below; the full output includes `expected_member_counts` for all member types.

Prompt 0 — Part 4:
Output JSON Schema (excerpt)

```

{
  "analysis": {
    "description": str,
    "stories": int,

```

```

"sections": [str, ...],
"roof_type":
"gable|hip|gambrel|shed",
"complexity":
"simple|moderate|complex",
"lot_size": { "width": float,
"depth": float, "area": float }
},
"sections": [{
"name": str,
"bounds": {
"x_min": float, "x_max": float,
"y_min": float, "y_max": float,
"z_base": float
},
"stories": int,
"systems":
["foundation", "floor", "walls", "roof"],
"dependencies": [str]
}],
"construction_order": [{
"step": int,
"section": str,
"phase": "foundation|floor|walls|roof",
"step_type": "critical|safe",
"members": [{ "type": str,
"count": int }],
"depends_on": [int]
}],
"expected_member_counts": {
"Sill": int, "Joist": int, ...
}
}

```

10.2. API Hyperparameters

Table 6 reports the API hyperparameters used for each model–protocol combination. All models use temperature = 0.0 to ensure deterministic outputs, except GPT-5 which does not expose a temperature parameter. The three protocols correspond to Planner-Atomic (Planner-Atomic, one-shot), Planner-Reactive (Planner-Reactive, hybrid cumulative), and Planner-Managed (Planner-Managed, stepwise). The iterative refinement with visual feedback pipeline uses the largest token budget (65,536) to accommodate full blend-file code revisions within a single API call.

Max retries under Planner-Managed. The stepwise protocol applies two retry limits: up to 5 retries *per step* if the partial structure falls below τ_{retry} , and a global cap of 30 retries across all steps per structure.

Context history. All three protocols maintain full conversation history during retries: each subsequent attempt receives all previous code outputs and structural validation error messages. For Planner-Atomic and Planner-Reactive, this is managed implicitly by the chat client, which accumulates the full `messages` list across attempts.

For Planner-Managed, history is managed by the `IterationController`, which exposes a `conversation_history_steps` parameter: Gemini retains the full construction transcript (999 steps), while GPT-5, Claude, and all other models truncate to the last 5 steps to prevent context overflow from accumulating per-step code outputs.

Render engine. The iterative refinement pipeline requires on-the-fly rendering at each feedback iteration; Cycles is used here to produce higher-fidelity images for the visual feedback signal. The visual similarity scores S_v reported across all protocols are also computed from Cycles renders to ensure a consistent comparison baseline.

11. Benchmark Construction Details

11.1. Blender Visualization

Figure 13 shows the 13 architectural style archetypes visualized in the Blender 3D viewport, which serve as the canonical massing templates for procedural dataset generation. The scene outliner for a representative ground-truth structure (RN_01_0119) illustrates the taxonomy-compliant member naming convention enforced across all 26,000+ structures in the dataset.

11.2. Compute Environment

All dataset generation, structural validation, and rendering were performed using **Blender 4.5.4 LTS** (build hash `b3efe983cc58`, commit `2025-10-27`) with the **Bonsai BIM** add-on for IFC-level structural metadata handling. Both tools are freely available open-source software.

Structural validation (the 10-test battery described in Section 7) is purely geometric and algebraic, it operates on member bounding boxes and graph connectivity, and requires no GPU. VLM API calls are likewise CPU-bound on the client

Table 6. API hyperparameters per model and protocol. τ_{retry} : visual similarity threshold below which the pipeline retries the current step or full generation. N/A: parameter not supported by the API. —: not applicable for this protocol.

Protocol	Model	Temp.	Max Tokens	Max Retries	τ_{retry}	Context History	Render Engine
Planner-Atomic	GPT-5	N/A	16,384	5	0.8	full	-
Planner-Atomic	Gemini	0.0	16,384	5	0.8	full	-
Planner-Atomic	Claude	0.0	16,384	5	0.8	full	-
Planner-Reactive	GPT-5	N/A	64,000	10	0.6	full	-
Planner-Reactive	Gemini	0.0	64,000	10	0.6	full	-
Planner-Reactive	Claude	0.0	64,000	10	0.6	full	-
Planner-Managed	GPT-5	N/A	16,384	5 / 30	0.4	full	-
Planner-Managed	Gemini	0.0	16,384	5 / 30	0.4	full	-
Planner-Managed	Claude	0.0	16,384	5 / 30	0.4	last 5	-
Iter. Refinement	GPT-5	N/A	65,536	10	0.6	full	Cycles
Iter. Refinement	Gemini	0.0	65,536	10	0.6	full	Cycles
Iter. Refinement	Claude	0.0	65,536	10	0.6	full	Cycles

side. GPU resources are used exclusively for Cycles rendering during the iterative refinement pipeline, where on-the-fly photorealistic renders are required as visual feedback at each iteration.

The pipeline is designed to be infrastructure-agnostic: the only hard dependency is a Blender installation accessible from the command line. No custom CUDA kernels, distributed training, or specialised hardware are required to reproduce the benchmark.

References

- [1] Claude opus 4.5. <https://www.anthropic.com/news/claude-opus-4-5>, 2025. 2, 9
- [2] Gemini 3 flash system card. <https://ai.google.dev/gemini-api/docs/models/gemini-3-flash-preview>, 2025. 2, 9
- [3] Qwen3.5-397b-a17b release. <https://huggingface.co/Qwen/Qwen3.5-397B-A17B>, 2026. 23
- [4] ACI Committee 318. *Building Code Requirements for Structural Concrete (ACI 318-19) and Commentary*. American Concrete Institute, Farmington Hills, MI, 2019. 19
- [5] Arash Adel, Andreas Thoma, Matthias Helmreich, Fabio Gramazio, and Matthias Kohler. Design of robotically fabricated timber frame structures. In *38th Annual Conference of the Association for Computer Aided Design in Architecture: Recalibration on Imprecision and Infidelity, ACADIA 2018*, pages 394–403. ACADIA, 2018. 4
- [6] Hassan Abu Alhaija, Jose Alvarez, Maciej Bala, Tiffany Cai, Tianshi Cao, Liz Cha, Joshua Chen, Mike Chen, Francesco Ferroni, Sanja Fidler, et al. Cosmos-transfer1: Conditional world generation with adaptive multimodal control. *arXiv preprint arXiv:2503.14492*, 2025. 2, 3
- [7] American Association of State Highway and Transportation Officials. *LRFD Bridge Design Specifications*. AASHTO, Washington, DC, 9th edition, 2020. 19
- [8] American Institute of Steel Construction. *Specification for Structural Steel Buildings (ANSI/AISC 360-22)*. AISC, Chicago, IL, 2022. 19
- [9] Yizhak Ben-Shabat, Jonathan Paul, Eviatar Segev, Oren ShROUT, and Stephen Gould. Ikea ego 3d dataset: Understanding furniture assembly actions from ego-view 3d point clouds. In *Proceedings of the IEEE/CVF Winter Conference on Applications of Computer Vision*, pages 4355–4364, 2024. 4
- [10] BIM Forum. *Level of Development (LOD) Spec-*

- ification Guide and Reference*, 2023. Accessed March 2026. 15
- [11] Shiqi Chen, Tongyao Zhu, Ruochen Zhou, Jinghan Zhang, Siyang Gao, Juan Carlos Niebles, Mor Geva, Junxian He, Jiajun Wu, and Manling Li. Why is spatial reasoning hard for vlms? an attention mechanism perspective on focus areas. *arXiv preprint arXiv:2503.01773*, 2025. 2
- [12] Yanzhe Chen, Kevin Qinghong Lin, and Mike Zheng Shou. Code2video: A code-centric paradigm for educational video generation. *arXiv preprint arXiv:2510.01174*, 2025. 3
- [13] Zhangquan Chen, Manyuan Zhang, Xinlei Yu, Xufang Luo, Mingze Sun, Zihao Pan, Yan Feng, Peng Pei, Xunliang Cai, and Ruqi Huang. Think with 3d: Geometric imagination grounded spatial reasoning from limited views. *arXiv preprint arXiv:2510.18632*, 2025. 2, 3
- [14] Wei Chow, Jiageng Mao, Boyi Li, Daniel Seita, Victor Guizilini, and Yue Wang. Physbench: Benchmarking and enhancing vision-language models for physical world understanding. In *ICLR*, 2025. 2, 3
- [15] Building Code. International residential code. *International Energy: Paris, France*, 2018. 3, 4
- [16] Jingtao Ding, Yunke Zhang, Yu Shang, Yuheng Zhang, Zefang Zong, Jie Feng, Yuan Yuan, Hongyuan Su, Nian Li, Nicholas Sukiennik, et al. Understanding world or predicting future? a comprehensive survey of world models. *ACM Computing Surveys*, 58(3):1–38, 2025. 2
- [17] Anna C Doris, Md Ferdous Alam, Amin Heyrani Nobari, and Faez Ahmed. Cad-coder: An open-source vision-language model for computer-aided design code generation. In *International Design Engineering Technical Conferences and Computers and Information in Engineering Conference*, page V03AT03A031. American Society of Mechanical Engineers, 2025. 3
- [18] Haoyi Duan, Hong-Xing Yu, Sirui Chen, Li Fei-Fei, and Jiajun Wu. Worldscore: A unified evaluation benchmark for world generation. In *Proceedings of the IEEE/CVF International Conference on Computer Vision*, pages 27713–27724, 2025. 2, 3
- [19] Chuan Fang, Heng Li, Yixun Liang, Jia Zheng, Yongsun Mao, Yuan Liu, Rui Tang, Zihan Zhou, and Ping Tan. Spatialgen: Layout-guided 3d indoor scene generation. In *International Conference on 3D Vision (3DV)*, 2026. 3
- [20] Jiaxin Ge, Zora Zhiruo Wang, Xuhui Zhou, Yi-Hao Peng, Sanjay Subramanian, Qinyue Tan, Maarten Sap, Alane Suhr, Daniel Fried, Graham Neubig, et al. Autopresent: Designing structured visuals from scratch. In *CVPR*, pages 2902–2911, 2025. 4
- [21] Yunqi Gu, Ian Huang, Jihyeon Je, Guandao Yang, and Leonidas Guibas. Blendergym: benchmarking foundational model systems for graphics editing. In *CVPR*, pages 18574–18583, 2025. 3
- [22] Roland Hess. *Blender foundations: The essential guide to learning blender 2.5*. Routledge, 2013. 4
- [23] Mengdi Jia, Zekun Qi, Shaochen Zhang, Wenyaoyao Zhang, Xinqiang Yu, Jiawei He, He Wang, and Li Yi. Omnispatial: Towards comprehensive spatial reasoning benchmark for vision language models. *arXiv preprint arXiv:2506.03135*, 2025. 3
- [24] Lingdong Kong, Wesley Yang, Jianbiao Mei, Youquan Liu, Ao Liang, Dekai Zhu, Dongyue Lu, Wei Yin, Xiaotao Hu, Mingkai Jia, et al. 3d and 4d world modeling: A survey. *arXiv preprint arXiv:2509.07996*, 2025. 2, 3
- [25] Hyun Joo Kwon, Hyun-Jeong Lee, and Julia O Beamish. Us boomers’ lifestyle and residential preferences for later life. *Journal of Asian Architecture and Building Engineering*, 15(2):255–262, 2016. 4
- [26] Youngwoon Lee, Edward S Hu, and Joseph J Lim. Ikea furniture assembly environment for long-horizon complex manipulation tasks. In *2021 IEEE International Conference on Robotics and Automation (ICRA)*, pages 6343–6349. IEEE, 2021. 4
- [27] Dacheng Li, Yunhao Fang, Yukang Chen, Shuo Yang, Shiyi Cao, Justin Wong, Michael Luo, Xiaolong Wang, Hongxu Yin, Joseph E Gonzalez, et al. Worldmodelbench: Judging video generation models as world models. *arXiv preprint arXiv:2502.20694*, 2025. 3
- [28] Ziyang Luo, Zhiqi Shen, Wenzhuo Yang, Zirui Zhao, Prathyusha Jwalapuram, Amrita Saha, Doyen Sahoo, Silvio Savarese, Caiming Xiong, and Junnan Li. Mcp-universe: Benchmarking large language models with real-world model context protocol servers. *arXiv preprint arXiv:2508.14704*, 2025. 3
- [29] José Marín, Tiffany MG Baptiste, Cristobal Rodero, Steven E Williams, Steven A Niederer, and Ignacio García-Fernández. Sciblend: Advanced data visualization workflows within blender. *Computers & Graphics*, 130:104264, 2025. 2
- [30] Nelson Nauata, Kai-Hung Chang, Chin-Yi Cheng, Greg Mori, and Yasutaka Furukawa. House-

- GAN: Relational generative adversarial networks for graph-constrained house layout generation. In *ECCV*, 2020. 17
- [31] Kun Ouyang, Yuanxin Liu, Haoning Wu, Yi Liu, Hao Zhou, Jie Zhou, Fandong Meng, and Xu Sun. Spacer: Reinforcing mllms in video spatial reasoning. *arXiv preprint arXiv:2504.01805*, 2025. 2
- [32] Zhenyu Pan and Han Liu. Metaspacial: Reinforcing 3d spatial reasoning in vlms for the metaverse. *arXiv preprint arXiv:2503.18470*, 2025. 2
- [33] Ye Peng, Ming Lu, and Ali Imanpour. Analysis of the rationality of extending lod standards from the design phase to the production and construction phases. In *International Conference on Computing in Civil and Building Engineering*, pages 314–324. Springer, 2024. 4
- [34] Ava Pun, Kangle Deng, Ruixuan Liu, Deva Ramanan, Changliu Liu, and Jun-Yan Zhu. Generating physically stable and buildable brick structures from text. In *Proceedings of the IEEE/CVF International Conference on Computer Vision*, pages 14798–14809, 2025. 3, 4
- [35] Fedor Rodionov, Abdelrahman Eldesokey, Michael Birsak, John Femiani, Bernard Ghanem, and Peter Wonka. Floorplanqa: A benchmark for spatial reasoning in llms using structured representations. *arXiv preprint arXiv:2507.07644*, 2025. 2, 3
- [36] Mohammad Amin Shabani, Sepidehsadat Hosseini, and Yasutaka Furukawa. HouseDiffusion: Vector floorplan generation via a diffusion model with discrete and continuous denoising. In *CVPR*, 2023. 17
- [37] Aaditya Singh, Adam Fry, Adam Perelman, Adam Tart, Adi Ganesh, Ahmed El-Kishky, Aidan McLaughlin, Aiden Low, AJ Ostrow, Akhila Ananthram, et al. Openai gpt-5 system card. <https://cdn.openai.com/gpt-5-system-card.pdf>, 2025. 2, 9
- [38] Ilias Stogiannidis, Steven McDonagh, and Sotirios A Tsafaris. Mind the gap: Benchmarking spatial reasoning in vision-language models. *arXiv preprint arXiv:2503.19707*, 2025. 2
- [39] Qiushi Sun, Jingyang Gong, Yang Liu, Qiaosheng Chen, Lei Li, Kai Chen, Qipeng Guo, Ben Kao, and Fei Yuan. Januscoder: Towards a foundational visual-programmatic interface for code intelligence. *arXiv preprint arXiv:2510.23538*, 2025. 3
- [40] Jiahao Tang, Henry Hengyuan Zhao, Lijian Wu, Yifei Tao, Dongxing Mao, Yang Wan, Jingru Tan, Min Zeng, Min Li, and Alex Jinpeng Wang. From charts to code: A hierarchical benchmark for multimodal models. *arXiv preprint arXiv:2510.17932*, 2025. 3, 4
- [41] Kexian Tang, Junyao Gao, Yanhong Zeng, Haodong Duan, Yanan Sun, Zhening Xing, Wenran Liu, Kaifeng Lyu, and Kai Chen. Lego-puzzles: How good are mllms at multi-step spatial reasoning? *arXiv preprint arXiv:2503.19990*, 2025. 2
- [42] HunyuanWorld Team, Zhenwei Wang, Yuhao Liu, Junta Wu, Zixiao Gu, Haoyuan Wang, Xuhui Zuo, Tianyu Huang, Wenhuan Li, Sheng Zhang, et al. Hunyuanworld 1.0: Generating immersive, explorable, and interactive 3d worlds from words or pixels. *arXiv preprint arXiv:2507.21809*, 2025. 2, 3
- [43] Ruocheng Wang, Yunzhi Zhang, Jiayuan Mao, Ran Zhang, Chin-Yi Cheng, and Jiajun Wu. Ikea-manual: Seeing shape assembly step by step. *Advances in Neural Information Processing Systems*, 35:28428–28440, 2022. 4
- [44] Xinjie Wang, Liu Liu, Yu Cao, Ruiqi Wu, Wenkang Qin, Dehui Wang, Wei Sui, and Zhizhong Su. Embodiedgen: Towards a generative 3d world engine for embodied intelligence. *arXiv preprint arXiv:2506.10600*, 2025. 2, 3
- [45] Junfei Wu, Jian Guan, Kaituo Feng, Qiang Liu, Shu Wu, Liang Wang, Wei Wu, and Tieniu Tan. Reinforcing spatial reasoning in vision-language models with interwoven thinking and visual drawing. *arXiv preprint arXiv:2506.09965*, 2025. 2
- [46] Bo Xia, Tim O’Neill, Jian Zuo, Martin Skitmore, and Qing Chen. Perceived obstacles to multi-storey timber-frame construction: an australian study. *Architectural science review*, 57(3):169–176, 2014. 4
- [47] Jianfeng Xiang, Zelong Lv, Sicheng Xu, Yu Deng, Ruicheng Wang, Bowen Zhang, Dong Chen, Xin Tong, and Jiaolong Yang. Structured 3d latents for scalable and versatile 3d generation. In *CVPR*, pages 21469–21480, 2025. 3
- [48] Jihan Yang, Shusheng Yang, Anjali W Gupta, Rilyn Han, Li Fei-Fei, and Saining Xie. Thinking in space: How multimodal large language models see, remember, and recall spaces. In *CVPR*, pages 10632–10643, 2025. 3
- [49] Weirui Ye, Fangchen Liu, Zheng Ding, Yang Gao, Oleh Rybkin, and Pieter Abbeel. Video2policy: Scaling up manipulation tasks in simulation through internet videos. *arXiv preprint arXiv:2502.09886*, 2025. 4

- [50] Guang Yin, Yitong Li, Yixuan Wang, Dale McConachie, Paarth Shah, Kunimatsu Hashimoto, Huan Zhang, Katherine Liu, and Yunzhu Li. Codediffuser: Attention-enhanced diffusion policy via vlm-generated code for instruction ambiguity. *arXiv preprint arXiv:2506.16652*, 2025. 3
- [51] Shaofeng Yin, Jiaxin Ge, Zora Zhiruo Wang, Xiuyu Li, Michael J Black, Trevor Darrell, Angjoo Kanazawa, and Haiwen Feng. Vision-as-inverse-graphics agent via interleaved multimodal reasoning. *arXiv preprint arXiv:2601.11109*, 2026. 3
- [52] Jirong Zha, Yuxuan Fan, Xiao Yang, Chen Gao, and Xinlei Chen. How to enable llm with 3d capacity? a survey of spatial reasoning in llm. *arXiv preprint arXiv:2504.05786*, 2025. 2
- [53] Weichen Zhang, Zile Zhou, Xin Zeng, Xuchen Liu, Jianjie Fang, Chen Gao, Yong Li, Jinqiang Cui, Xinlei Chen, and Xiao-Ping Zhang. Open3d-vqa: A benchmark for comprehensive spatial reasoning with multimodal large language model in open space. *arXiv preprint arXiv:2503.11094*, 2025. 2, 3
- [54] Yifan Zhang, Chunli Peng, Boyang Wang, Puyi Wang, Qingcheng Zhu, Fei Kang, Biao Jiang, Zedong Gao, Eric Li, Yang Liu, et al. Matrix-game: Interactive world foundation model. *arXiv preprint arXiv:2506.18701*, 2025. 3
- [55] Zhengxue Zhou, Satheeshkumar Veeramani, Hatem Fakhruddin, Seda Uyanik, and Andrew I Cooper. Genco: A dual vlm generate-correct framework for adaptive peg-in-hole robotics. In *2025 IEEE International Conference on Robotics and Automation (ICRA)*, pages 16744–16751. IEEE, 2025. 3